TU Delft

Delft University of Technology

Document Version
Final published version

Licence
CC BY-NC

Citation (APA)
Ripamonti, A., Lacassin, M., Droghetti, R., Bokinsky, G., & Cosentino Lagomarsino, M. (2026). Transcriptional competition biases the effects of second messengers in Escherichia coli. *Cell Systems*, *17*(6), Article 101609. https://doi.org/10.1016/j.cels.2026.101609

Important note
To cite this publication, please use the final published version (if applicable).
Please check the document version above.

Copyright
In case the licence states “Dutch Copyright Act (Article 25fa)”, this publication was made available Green Open Access via the TU Delft Institutional Repository pursuant to Dutch Copyright Act (Article 25fa, the Taverne amendment). This provision does not affect copyright ownership.
Unless copyright is transferred by contract or statute, it remains with the copyright holder.

Sharing and reuse
Other than for strictly personal use, it is not permitted to download, forward or distribute the text or part of it, without the consent of the author(s) and/or copyright holder(s), unless the work is under an open content license such as Creative Commons.

Takedown policy
Please contact us and provide details if you believe this document breaches copyrights.
We will remove access to the work immediately and investigate your claim.

This work is downloaded from Delft University of Technology.

Cell Systems

Article

Transcriptional competition biases the effects of second messengers in *Escherichia coli*

Graphical abstract

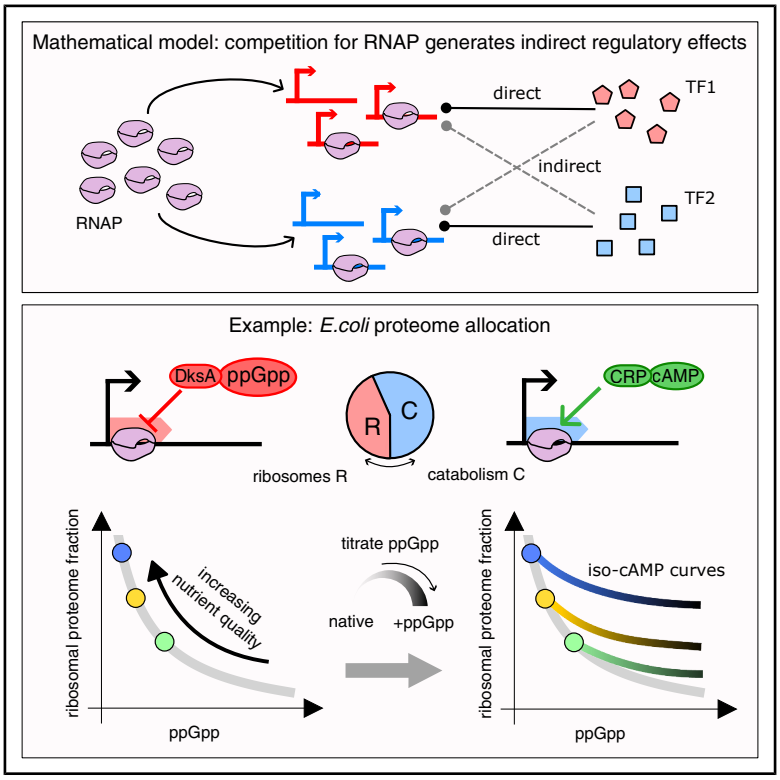

Highlights

- Mathematical modeling links proteome allocation to global transcriptional limits
- Shared transcriptional resources connect ppGpp and cAMP signaling in *E. coli*
- ppGpp titration exposes proteome-level effects of transcriptional coupling
- Data and models show ribosome expression is not controlled by ppGpp alone

Authors

Andrea Ripamonti, Milan Lacassin, Rossana Droghetti, Gregory Bokinsky, Marco Cosentino Lagomarsino

Correspondence

marco.cosentino-lagomarsino@ifom.eu

In brief

Regulator-promoter interactions are often studied in isolation. Ripamonti, Lacassin, et al. demonstrate that indirect regulatory effects can arise through competition for shared transcriptional resources. Focusing on bacterial second messengers, they show cAMP can affect ppGpp targets, highlighting that gene expression is influenced by more than direct regulators.

Ripamonti et al., 2026, Cell Systems *17*, 101609
June 17, 2026 © 2026 The Authors. Published by Elsevier Inc.
https://doi.org/10.1016/j.cels.2026.101609

CellPress

Cell Systems

CellPress
OPEN ACCESS

Article

Transcriptional competition biases the effects of second messengers in *Escherichia coli*

Andrea Ripamonti,[1,2,5] Milan Lacassin,[3,5] Rossana Droghetti,[2] Gregory Bokinsky,[3,6] and Marco Cosentino Lagomarsino[1,2,4,6,7,*]

[1]Dipartimento di Fisica, Università degli Studi di Milano, via Celoria 16, Milan, Italy
[2]IFOM ETS - The AIRC Institute of Molecular Oncology, via Adamello 16, Milan, Italy
[3]Department of Bionanoscience, Kavli Institute of Nanoscience, Delft University of Technology, Delft, the Netherlands
[4]INFN Sezione di Milano, via Celoria 16, Milan, Italy
[5]These authors contributed equally
[6]These authors contributed equally
[7]Lead contact
*Correspondence: marco.cosentino-lagomarsino@ifom.eu
https://doi.org/10.1016/j.cels.2026.101609

SUMMARY

Cells regulate gene expression by balancing transcriptional resources across different functional groups of genes. In *Escherichia coli*, second messengers such as ppGpp and cAMP control ribosome biogenesis and metabolic gene expression, respectively. While these regulators are typically studied in isolation, we provide a theory showing that their effects are intertwined as a result of global transcriptional competition. Using experimental data from RelA overexpression and a mechanistic modeling framework, we show that ppGpp-mediated repression of ribosomal genes competes for transcriptional resources with cAMP-driven activation of catabolic genes. This competition reshapes proteome allocation in a way that transcends individual regulators. Our findings challenge common modeling assumptions about transcription factor action and revive classical ideas suggesting that large-scale gene regulation should be studied within the broader context of resource availability, with implications for understanding cellular regulation across diverse biological systems beyond bacterial physiology.

INTRODUCTION

Precise regulation of gene expression is fundamental to cellular physiology, with implications for fitness and disease.[1–4] For instance, cells respond to growth limitations by expressing ribosomes and enzymes required to balance the supply and demand of key metabolites.[5] In this context, the proteome sector theory has emerged, particularly in *Escherichia coli*,[6–10] as a powerful mathematical approach that captures large-scale gene regulatory principles due to mass balance and supply-demand, including the well-established linear relationship between ribosomal content and growth rate (sometimes termed the "ribosomal growth law"[6,11]). Recent advances in proteomics have further refined our understanding of proteome allocation, revealing how cells can prioritize protein synthesis in response to environmental conditions and the internal state.[8,9,12–15]

A crucial open question is how cells integrate environmental signals and internal sensing to regulate ribosomal allocation and change the growth rate. One key mechanism for growth rate control in *E. coli* involves the alarmone (p)ppGpp (henceforth shortened as ppGpp), a global regulator of the ribosomal protein sector.[1] Together with the transcription factor DksA, ppGpp binds to RNA polymerase (RNAP), inducing a conformational change that inhibits the transcription of genes encoding ribosomal RNA and proteins.[16–19] Additionally, ppGpp has many intracellular targets potentially linked to metabolism and translation, but the transcriptional effect appears to be dominant for ribosome regulation.[16]

Recent work by Wu et al.[20] demonstrated that ppGpp levels quantitatively reflect translation elongation rates, establishing a direct link between the cellular perception of growth rate and ribosomal biogenesis. Mechanistically, ppGpp is synthesized from GTP by the ribosome-bound enzyme RelA when uncharged tRNAs bind to the ribosomal A site.[21–23] The enzyme SpoT also has a limited capacity for ppGpp synthesis, though its main role is as a ppGpp hydrolase.[24] Thus, under starvation, ppGpp acts as a sensor of nutrient availability and redirects resources from the translation machinery toward metabolism.[25,26]

Just as cellular resources must be efficiently allocated at the protein level, transcription itself requires careful distribution of RNAP across different genes. The limited transcriptional capacity of the RNAP pool represents a fundamental constraint on gene expression, analogous to the limited proteome capacity.[27–29] This constraint means that increased transcription of one gene or set of genes necessarily affects the expression of others through competition for RNAP. While traditional views

This is an open access article under the CC BY-NC license (http://creativecommons.org/licenses/by-nc/4.0/).

of transcriptional regulation focus on individual promoter-regulator interactions, the allocation of RNAP across different promoters emerges as a critical systems-level consideration, particularly when examining large-scale changes in gene expression such as those involving entire proteome sectors.[30,31]

This perspective suggests that global regulators like ppGpp might coordinate cellular responses not only through direct promoter interactions but also by influencing the competition for RNAP allocation across the genome. Thus, their effect should depend on the contextual activity of other global regulators. One such example is the second messenger cyclic AMP (cAMP), a small molecule that modulates metabolic gene expression in response to the availability of carbon substrates.[32,33] Despite their distinct roles, both ppGpp and cAMP influence proteome allocation at the transcriptional level, shaping the ribosomal and metabolic sectors in response to nutrient availability. While specific crosstalk between (p)ppGpp and other nucleotide messengers is being explored,[34] including signal conversion, allosteric regulation, and target competition, competition for RNAP allocation has comparatively received less attention.

Perturbing these second messengers by "opening the loops" of feedback control[35,36] provides a powerful strategy to address this gap, allowing us to test our understanding of transcriptional regulation and gain key insights into regulatory interactions. For instance, Zhu and Dai[37] explored the effects of ppGpp overabundance by overexpressing its synthase enzyme, RelA, demonstrating that the ribosomal growth law is robust, despite broad proteomic rearrangements.[38,39] Similarly, Kochanowski et al.[40] showed that cAMP titration preserves the same growth law. While these findings highlight the robustness of the ribosomal growth law, they also raise fundamental questions about the mechanisms governing proteome allocation under these perturbations. Intriguingly, prior studies suggest that the link between ppGpp and the growth rate is not univocal, particularly when RelA is overexpressed.[41–43] This divergence (reviewed in Imholz et al. [44]) has so far remained unexplained and challenges the prevailing framework, suggesting a more complex interplay between ppGpp, global transcriptional regulation, and growth rate control.

Although recent models offer promising steps toward a mechanistic theory of proteome allocation, key gaps remain. Existing theories that connect proteome sectors with nutrient and growth sensing often overlook the mechanistic details of transcription.[36,45,46] Recent studies by Balakrishnan et al.[31] and by Lin and Amir[27] provide a solid foundation for describing the flow of information from DNA to proteins, yet they are not fully embedded within the proteome sector framework. Conversely, the model proposed by Calabrese et al.[29] incorporates transcription and translation but lacks the regulatory details needed to capture the effects of second messengers.

In this work, we address the limitations of existing theories by adopting a theory-first approach. Building on the study of Balakrishnan et al.[31], we develop a framework that integrates transcriptional regulation by second messengers and competition for RNAPs into proteome sector models. This framework enables a model-guided analysis of experimental data. Leveraging published datasets from Wu et al.,[20] Balakrishnan et al., [31] Zhu and Dai,[37] Zhu and Dai,[38] Zhu et al.,[39] and Dai et al.,[47] as well as performing new experiments involving RelA overexpression, we investigate a previously uncharacterized divergence in the relationship between ppGpp and ribosomal content. By simultaneously monitoring the levels of ppGpp and cAMP, we uncover non-trivial effects of second messengers on proteome coordination. These effects are effectively captured by our model, which describes second messenger-regulated transcriptional competition between proteome sectors.

RESULTS

Global transcriptional coupling connects differentially regulated proteome sectors

Building on the framework of Balakrishnan et al.,[31] we introduce a model that integrates transcriptional regulation by second messengers and competition for RNAPs into proteome sector dynamics (see Methods S1 for detailed derivations and assumptions). We denote the mass fraction of each proteome sector I as

$$\phi_I = \frac{M_I}{M} \qquad \text{(Equation 1)}$$

where M_I is the total mass of proteins in sector I, and M is the total protein mass. For example, the "ribosomal sector" (ϕ_R) includes proteins involved in translation, while other sectors, such as metabolic (ϕ_P) and housekeeping (ϕ_Q), are categorized based on their response to growth limitations.[6,8,9,33]

The model focuses on how mRNAs from different sectors are produced. We define the "transcriptome fraction" χ_I as the fractional proportion of mRNAs encoding proteins in sector I. Assuming no post-transcriptional regulation, the time evolution of protein mass fractions is given by (Methods S1 for derivation)

$$\frac{d\phi_I}{dt} = \epsilon f_a \phi_R (\chi_I - \phi_I) \qquad \text{(Equation 2)}$$

where ϵ is the translation elongation rate, f_a is the fraction of active ribosomes, and the product $\epsilon f_a \phi_R$ corresponds to the growth rate λ.

Transcript dynamics are described in an "initiation-limited" regime,[31,48] where the concentration of a transcript species $[m_i]$ evolves as

$$\frac{d[m_i]}{dt} = \alpha_i [G_i] - (\delta + \lambda)[m_i]. \qquad \text{(Equation 3)}$$

Here α_i is the transcription initiation rate, δ is the uniform mRNA degradation rate, and $[G_i]$ is the gene concentration. The dilution term $-\lambda[m_i]$ accounts for the time variation in cellular volume. Initiation rates depend on the concentration of available RNAP holoenzymes $[N_{av}]$, and are given by

$$\alpha_i = k_i [N_{av}] \qquad \text{(Equation 4)}$$

where k_i is the promoter strength, influenced by transcriptional regulators (Figure 1A).

Balakrishnan et al.[31] found that holoenzyme formation is limited by sigma factors, mainly by the housekeeping RpoD (σ^{70}), rather than by RNAP core components. Therefore, as a first approximation, the above equation can be interpreted as reflecting the assumption of σ^{70}-limited transcription initiation. Although the model can be extended to incorporate alternative

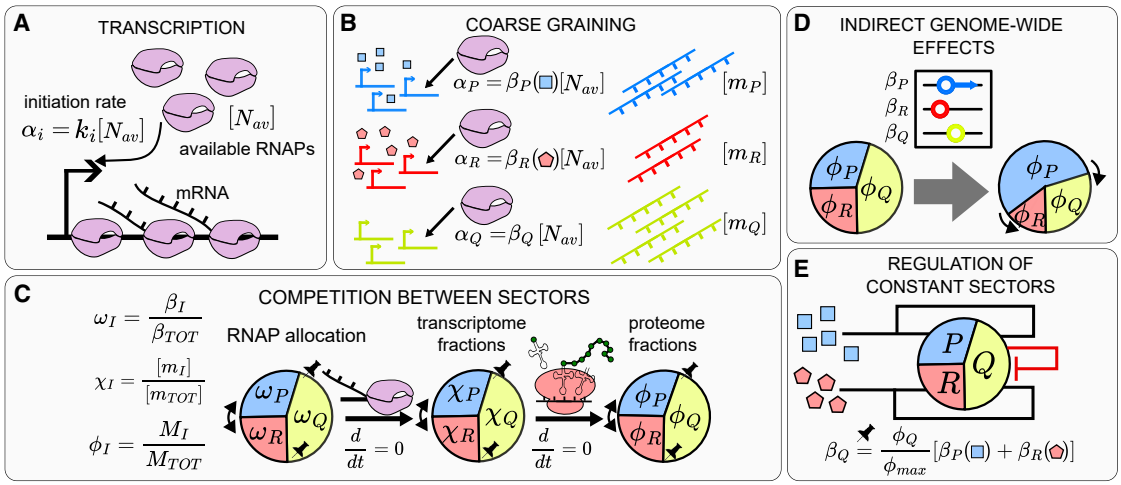

Figure 1. Illustration of the model for transcriptional competition and its features

(A) Transcription initiation rates are proportional to the concentration of available RNA polymerases $[N_{av}]$ (the model neglects traffic of RNA polymerase on genes).

(B) Genes are grouped into sectors (three in this illustration). The R and P sectors are controlled by regulators, which act on the "sector strengths" β_R and β_P at the transcriptional level. mRNA abundances $[m_I]$ are determined by the coarse-grained initiation rates α_I.

(C) Sector strengths determine the transcriptome fractions χ_I. The Q sector is assumed to be regulated in such a way that ϕ_Q is "pinned" at a constant value across conditions. At steady-state, transcriptome fractions correspond to proteome fractions ϕ_I.

(D) Due to the normalization constraint, activation or repression of a single sector indirectly affects all others, even if their sector strengths remain unchanged.

(E) Maintaining a constant Q sector size requires direct regulation, influenced either by signals coupled to the R and P sectors (black arrows) or by negative autoregulation (red T-shaped arrow), ensuring homeostasis.

sigma factors (Methods S1), we do not expect them to substantially affect our main results (see discussion). Similarly, while core RNAP abundance can be described with a dedicated proteome sector,[27–29] our simplified framework does not rely on it. We emphasize that a non-RNAP-limited regime is possible,[49] but it falls outside the scope of this study, since in this regime transcription output per gene is constant and total mRNA scales directly with the number of promoters.[27]

The key novelty of our approach lies in embedding transcription into proteome sector theory by introducing sector-specific coarse-grained promoter strengths β_I (Figure 1B). This allows us to express mRNA dynamics at the sector level,

$$\frac{d[m_I]}{dt} = \alpha_I[G] - (\delta + \lambda)[m_I], \qquad \text{(Equation 5)}$$

where we defined the "coarse-grained initiation rate" $\alpha_I = \beta_I[N_{av}]$ and the typical gene concentration $[G]$, which we assume to be uniform across all sectors (see STAR Methods and Methods S1 for a model variant including gene dosage effects). From this, we derive the time evolution of transcriptome fractions χ_I (Methods S1),

$$\frac{d\chi_I}{dt} = \frac{1}{\tau_\chi}(\omega_I - \chi_I), \qquad \text{(Equation 6)}$$

where $\omega_I = \frac{\beta_I}{\beta_{TOT}}$ represents RNAP allocation across sectors, with $\beta_{TOT} = \sum_J \beta_J$, while τ_χ is a characteristic relaxation timescale.

In steady-state growth, our model predicts that proteome fractions are determined transcriptionally by sector "strengths" (Figure 1C) as follows:

$$\phi_I = \chi_I = \omega_I = \frac{\beta_I}{\sum_J \beta_J} \qquad \text{(Equation 7)}$$

This relationship, proposed for single genes in Balakrishnan et al.[31], implies that transcriptional regulation in one sector indirectly affects other sectors due to the normalization condition $\sum_I \omega_I = 1$ (Figure 1D). This coupling is central to our framework, since it sets how global transcriptional regulation and competition for RNAPs shape proteome coordination.

Sectors with constant size must be actively maintained at a fixed expression level

To understand the role played by transcriptional competition in setting the sizes of different sectors, we focused on a commonly used three-sector model.[6,7,36] This model typically assumes that the mass fraction ϕ_Q of the housekeeping sector remains constant.[6] We incorporate this constraint into our framework using Equation 7, finding

$$\beta_Q = \frac{\phi_Q}{\phi_{max}}(\beta_R + \beta_P)$$
$$\phi_R = \frac{\beta_R}{\beta_P + \beta_R}\phi_{max}. \qquad \text{(Equation 8)}$$

Since sectors P and R are regulated in order to adapt to different conditions (e.g., different nutrients), the sum $\beta_P + \beta_R$ varies with the regulation, thus β_Q must follow its behavior in a proportional way (Figure 1E). The second identity in Equation 8 describes the competition between the P and R sectors for a proteome fraction equal to $\phi_{max} = 1 - \phi_Q$. Note that Equation 8 strictly applies only at steady-state. In addition, the

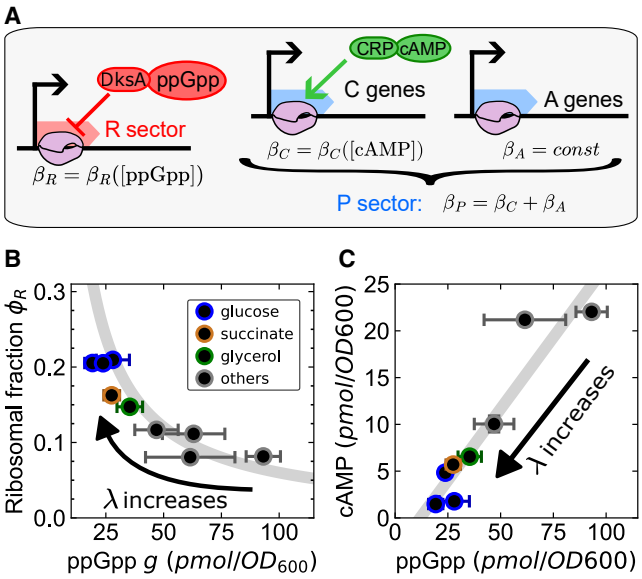

Figure 2. A positive covariation of ppGpp and cAMP under catabolic limitation defines proteome allocation as a function of ppGpp

(A) The model for transcriptional competition in *E. coli* describes the ribosomal (R) sector as repressed by ppGpp-DksA. This sector competes with the catabolic (C) sector, activated by cAMP-Crp, and with a constitutive (unregulated) anabolic (A) sector. C and A sectors form the P sector.

(B) Under catabolic limitation, the ribosomal fraction ϕ_R decreases with increasing ppGpp. The plot derives from our direct measurements of ppGpp levels and growth rate. Values for the ribosomal fraction are estimated from growth rate using joint measurements of RNA/protein ratio and growth rate from Zhu and Dai.[37] The gray line represents the best fit according to the expression $\phi_R \propto \frac{1}{g}$ as in Wu et al.[20]

(C) Under catabolic limitation, cAMP increases approximately linearly with ppGpp (and therefore with decreasing growth rate) in the wild type (gray line, best fit). This correlation obscures the specific effect of cAMP on ϕ_R when considered solely as a function of ppGpp. Error bars represent standard error across technical replicates.

first relationship does not necessarily imply that the Q sector shares transcriptional regulators with the other two sectors. For instance, some studies[6,30,50] have proposed that this sector maintains its constant size through negative autoregulation. Proteomics studies[8,9] indicate that Q consists of multiple subsectors, each responding differently to growth limitations, while their overall sum remains constant. Regardless of the specific mechanisms governing Q, Equation 8 provides the shape of its mean regulatory function in terms of β_P and β_R.

A positive covariation of ppGpp and cAMP coordinates proteome allocation under catabolic limitation

With a constant Q sector, proteome allocation is entirely determined by the relative sizes of R and P from Equation 8, and ppGpp is believed to be a central driver of this process[16,21,51] (Figure 2A). To confirm this, we directly measured internal ppGpp levels in combination with growth rate across multiple conditions, corresponding to different carbon sources (see STAR Methods). We converted growth rate data into ribosomal fractions using the linear ribosomal growth law.[6] Consistent with the literature,[20,37,41,52] we observed a robust relationship between ϕ_R and g (*ppGpp concentration*), with elevated ppGpp levels corresponding to slower growth rates, and thus smaller ribosomal fractions (Figure 2B).

With only three proteome sectors, incorporating a passive P sector is sufficient to account for this growth rate-dependent proteome partitioning, consistent with the original suggestion by Scott et al.[6] Under these assumptions, the steady-state proteome composition is a function of ppGpp only: $\phi_R = \phi_R(g)$ and $\phi_P = \phi_P(g)$. Models with ppGpp as the sole transcriptional regulator are commonly found in the literature,[20,36,45] because this minimal setup effectively captures the correlation between ϕ_R and g across nutrient conditions seen in various *E. coli* studies.

However, previous studies[1,33,40,53–55] show the importance of the second messenger cAMP as a global regulator. cAMP activates the transcription factor CRP (cAMP receptor protein), which in turn drives catabolic gene expression by binding specific DNA sequences and interacting with the α subunit of RNAP.[32,56,57] Produced by adenylate cyclase (Cya), cAMP levels depend on carbon substrate availability. You et al.[33] proposed that Cya activity is repressed by alpha-keto acids (e.g., oxaloacetate), forming a feedback loop: when alpha-keto acids accumulate, cAMP synthesis and catabolic gene expression are downregulated, allowing *E. coli* to adjust its metabolism according to nutrient availability. Given that cAMP-CRP regulates hundreds of genes,[58,59] and that catabolic proteins can represent up to 30% of the cellular proteome under certain conditions[40] (comparable with the ribosomal sector in rich media), we reasoned that this regulator could exert effects at the global cellular scale and should not be neglected.

According to You et al.,[33] catabolic proteins form a subsector of the P sector, which is complemented by the anabolic subsector. The catabolic sector strength, β_C, can be expressed as a function of cAMP concentration (denoted by c), $\beta_C = \beta_C(c)$ (Figure 2A). The anabolic component can be considered as passive (i.e., constitutive) to a first approximation,[40] with a constant strength β_A. While alternative proteome partitions are possible,[6,53,60] a fundamental assumption relevant to our study is that a large part of the P sector is activated by cAMP. Therefore, we can write $\beta_P = \beta_C(c) + \beta_A = \beta_P(c)$, while for the R sector we can set $\beta_R = \beta_R(g)$. Thanks to Equation 8 we obtain, at steady-state:

$$\phi_R(g,c) = \frac{\beta_R(g)}{\beta_R(g)+\beta_P(c)}\phi_{max} = \left[1+\frac{\beta_P(c)}{\beta_R(g)}\right]^{-1}\phi_{max} \quad \text{(Equation 9)}$$

Crucially, ϕ_R becomes a function of both ppGpp and cAMP concentrations. The strong variation of ϕ_R with g in wild-type data can be explained in two ways: either cAMP signaling plays a minor role compared with ppGpp regulation, or cAMP levels vary jointly with ppGpp as a function of growth rate, $c = c(g)$. To distinguish between these scenarios, we measured cAMP levels under the same conditions as in Figure 2B using the same methodology as for ppGpp. Consistent with the second hypothesis, we observed that ppGpp and cAMP levels covary, with their relation approximately linear (Figure 2C). As ppGpp levels increase, repressing the R sector, cAMP concentrations rise concurrently, activating the P sector. This coordinated response ensures that both cAMP and ppGpp collectively redirect resources from translation to metabolism, reflecting a joint modulation of proteome allocation by these second messengers. Notably, our model does not

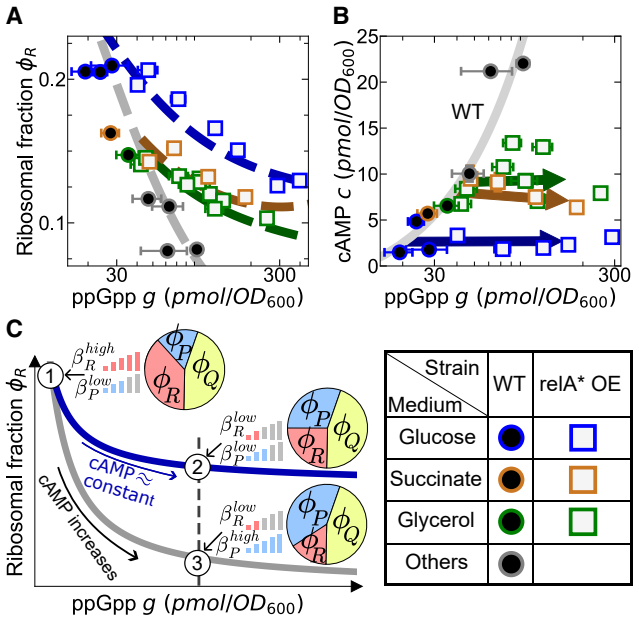

Figure 3. Lack of cAMP target activation under RelA overexpression attenuates ppGpp-mediated ribosomal repression via transcriptional competition, falsifying competition-free models

(A) Upon RelA overexpression (squares), the wild-type relation between ϕ_R and ppGpp (circles) breaks down. By a proper choice of the functions $\beta_R(g)$ and $\beta_P(c)$, the model reproduces both wild-type (gray dashed line) and RelA overexpression data (colored dashed lines). To visualize the model's predictions, we assumed that cAMP levels vary linearly with ppGpp changes during RelA overexpression (see STAR Methods), as indicated by the arrows in Figure 3B.

(B) The WT relation between ppGpp and cAMP (solid gray line, same as in Figure 2C, but in log scale) is broken when overexpressing RelA. For a fixed carbon source, cAMP levels vary only minimally with increasing ppGpp. Arrows indicate the linear fits used as input for the model predictions in (A).

(C) Origin of the branching in Figure 2A. At low ppGpp (1), ribosomal promoters operate at maximal capacity, while the P sector is minimally activated. If RelA is overexpressed starting from this condition (blue line), R is repressed by the increased ppGpp concentration, but the intrinsic activation of the P sector remains approximately constant due to unchanged cAMP levels (2). Conversely, if the same ppGpp concentration is achieved in the wild type by worsening the nutrient quality (gray line), cAMP levels rise and activate the P sector. This results in a smaller ribosomal fraction in the latter case (3). Error bars represent standard error across technical replicates.

assume any causal relationship between ppGpp and cAMP, nor do our data provide direct evidence for causality; for further considerations on potential interpretations, we refer to the discussion section. We also emphasize that this positive correlation is observed specifically under catabolic limitation (C-LIM), where growth is restricted by changing the carbon source. However, our model predicts that different behaviors may emerge under other perturbations (see below).

RelA overexpression reveals indirect regulation of ribosomal proteins by transcriptional competition with cAMP targets

Having established that ppGpp and cAMP covary positively under C-LIM, we reasoned that perturbations in ppGpp levels could disentangle this correlation and reveal the effects of transcriptional competition. To test this, we titrated ppGpp by overexpressing the N-terminal catalytic domain of the enzyme RelA (referred to as RelA*) using an inducible TetR-pTet system. We measured steady-state growth rate together with ppGpp and cAMP concentrations at different degrees of induction, and with different carbon sources as supplements (see STAR Methods).

Previous studies have explored RelA* overexpression and provided key insights that inform our analysis. Firstly, this perturbation is known to reduce the steady-state growth rate,[37,41,61] a finding confirmed in our data (Figure S1). As mentioned in the introduction, Zhu and Dai.[37] demonstrated that this decrease in growth rate is also associated with a reduction in rRNA content (a proxy for the ribosomal fraction[6]), whereas the relationship between the two (the ribosomal growth law) remains unchanged (Figure S2). Based on this observation, we are able to convert growth rates into ribosomal fractions with the same coefficients used for the unperturbed conditions (STAR Methods).

As mentioned in the introduction, earlier work[41–44] suggested that the relationship between growth rate λ and ppGpp g breaks under RelA overexpression; therefore, the relationship between the ribosomal sector and ppGpp, which is central to wild-type physiology (Figure 2B), must also be broken. This is noteworthy, as one might expect that elevating ppGpp levels in RelA overexpression mutants would simply shift cells to a slower growth regime, while still maintaining the wild-type $g - \phi_R$ correlation. However, our measurements confirm that the relationship between ϕ_R and g is not conserved (Figure 3A).

Specifically, at equivalent ppGpp concentrations, RelA* overexpression mutants, despite an overall decrease in their growth, displayed higher growth rates, and hence higher ribosomal fractions, compared with the wild type (Figures 3A and S1). In other words, RelA* overexpression reduces the repressive power of ppGpp on ribosome biogenesis, as the same ppGpp concentrations give higher ribosomal levels than in unperturbed conditions. Similarly, this conclusion is supported by comparing recent data from Zhu and Dai[38] and Zhu et al.[39] with our wild-type data (Figure S2).

Thus, our observations support the idea that ribosomal content is not solely dependent on ppGpp levels. This challenges regulatory models that propose ppGpp as the exclusive regulator of proteome partitioning. Instead, our findings support a more complex scenario involving competition for RNAP between multiple large-scale gene expression programs, described by our model through Equation 9.

To further explore this deviation, we examined the relation between ppGpp and cAMP under RelA overexpression. Remarkably, cAMP concentration data points fall below, rather than on, the wild-type ppGpp-cAMP curve (Figure 3B). This implies that, at the same ppGpp concentration, the catabolic sector is less activated by cAMP compared with the physiological level of activation found in the wild-type strain. The trend in cAMP data is in line with a constant for growth in minimal medium supplemented with glucose (blue arrow), and is compatible with a constant for minimal medium supplemented with succinate (ochre arrow). For these two conditions, we can reasonably conclude that cAMP levels remain largely unaffected by RelA overexpression. The behavior observed in glycerol is more complex, yet cAMP levels still remain below the wild-type curve (gray line).

Based on these observations, we determined the functional shapes of the two sector strengths β_P and β_R required for the model to reproduce our data for both the wild type and RelA* overexpression mutants. Using Equation 9, we found that a model with

$$\beta_P(c) = \rho\left[\mu_1\left(1+\frac{c}{\mu_2}\right)\right]$$
$$\beta_R(g) = \rho\left[1+\frac{\mu_3}{g}\right] \quad \text{(Equation 10)}$$

reproduces the data well (see Figure S3A for an estimate of the goodness of fit), where μ_1, μ_2, and μ_3 can be fixed by fitting (Table S1) and ρ remains a free parameter. The predictions of the model can be visualized as a function of ppGpp by assuming a relationship between cAMP and ppGpp for each carbon source. Figure 3A shows the outcome assuming the best linear fits, represented by arrows in Figure 3B. Other representations of the cAMP-ppGpp relationship lead to slightly different visualization in the $g - \phi_R$ plane (Figures S3B and S3C) without impacting the quality of the fit.

While this model is fairly rich in parameters, it gives rise to simple interpretations. The parameters μ_2 and μ_3 are, respectively, effective cAMP and ppGpp concentrations. The parameter μ_1 accounts for different number of genes and basal promoter strengths between the two sectors. A basal rate for the R sector is necessary because extreme ppGpp overabundance does not reduce the ribosomal fraction to the lowest levels observed in the wild type; instead, ϕ_R appears to approach an asymptotic value, particularly for glucose and glycerol (Figure 3A, high ppGpp region). The basal rate for P reflects the contribution from its anabolic subsector[40] (see discussion for details).

The model also necessarily includes the free parameter ρ, because our approach is only able to access the *ratio* $\frac{\beta_P}{\beta_R}$ (see Equation 9). Therefore, the model is invariant with respect to scaling both activities by a common multiplicative factor, which potentially keeps into account transcriptional effects shared by the two sectors, as well as the potential influence of ppGpp on Crp activity[62] (discussion and Methods S1). For simplicity, we assume the absence of such effects, treating ρ as a constant. However, even if these effects were present, we note that ρ would only affect the total promoter strength β_{TOT}, without influencing competition between the R and P sectors, which is fully determined by the effective concentrations μ_2 and μ_3.

We can illustrate the key features of the model using glucose as a reference condition (Figure 3C). In wild-type cells growing on glucose, ppGpp and cAMP levels are low: this leads to strong derepression of the R sector and a lack of activation of the P sector, resulting in a high ribosomal fraction, $\phi_{R,1} = \frac{\beta_R^{high}}{\beta_R^{high}+\beta_P^{low}}\phi_{max}$. When ppGpp increases due to RelA overexpression (blue line in Figure 3C) while keeping glucose as the carbon source, it represses the R sector. However, because cAMP levels remain constant, the P sector is not activated, leading to only a small reduction in ribosome abundance, with $\phi_{R,2} = \frac{\beta_R^{low}}{\beta_R^{low}+\beta_P^{low}}\phi_{max}$. In contrast, when ppGpp increases to the same value due to worsened nutrient quality (gray line in Figure 3C), cAMP levels rise in tandem, activating the P sector and resulting in a more significant downregulation of the ribosomal sector, with $\phi_{R,3} = \frac{\beta_R^{low}}{\beta_R^{low}+\beta_P^{high}}\phi_{max} < \phi_{R,2}$. Note that this reasoning also applies when cAMP levels are not constant under RelA overexpression, as long as they remain below the wild-type cAMP-ppGpp curve, as seen in glycerol (green squares in Figure 3B).

Thus, the relationship between ppGpp and R sector expression observed in wild-type conditions is not only a consequence of ppGpp repression but also a result of transcriptional competition (or equivalently, a competition for allocation of free RNAP) with catabolic genes, which are activated by cAMP. In contrast, during RelA* overexpression, the relationship between ppGpp and R sector expression reflects ppGpp repression alone, without concomitant activation of catabolism. Therefore, repression of the ribosomal sector appears weaker in this condition, as higher ppGpp levels are required to suppress ribosomal protein expression compared with wild-type conditions.

This is the central result of our study: R sector expression is determined not only by ppGpp concentration but also by constraints imposed by RNAP allocation and transcriptional competition with other sectors.

Alternative explanatory models require transcriptional competition between sectors

To assess the robustness of our findings, we explored various alternative models to account for potential confounding factors that could contribute to the observed data. One such factor is gene-dosage-dependent effects, which are not explicitly included in the simplest version of our framework. While we present a method to address these in the Methods S1 document, we briefly note here that the growth rate dependence of the ori/ter ratio, which determines copy numbers, remains unchanged under ppGpp overabundance.[63] Building on this, we show that gene copy number variations do not account for the divergence in the relationship between ϕ_R and g (Methods S1). Within the examined growth rate range, these effects are minimal, and incorporating them into our fitting algorithm results only in parameter adjustments (Table S1). Moreover, we note that the branching in Figure 3A is not caused by variations in the rate of replication initiation, which may be under complex regulation.[63] This is because our definition of regulatory functions is independent of Ori concentration, which influences total gene concentrations, but not relative levels. Additionally, it is important to emphasize that our model is independent of the speed of transcriptional elongation or cell size, variables that are both known to be affected by RelA overexpression,[52,61] but are not related to transcriptional competition.

In addition, considering the mechanisms of ppGpp-dependent repression of ribosomal genes, attention should be given to the role of DksA, which is required for ppGpp activity as a transcriptional repressor of the ribosomal sector. One might propose that ppGpp-mediated repression becomes limited by DksA under high ppGpp levels. However, data from Mori et al.[9] and Paul et al.[64] show that, in the wild type, DksA is maintained at a constant level across perturbations, which likely reflects negative autoregulation of its gene.[65] Therefore, we can safely

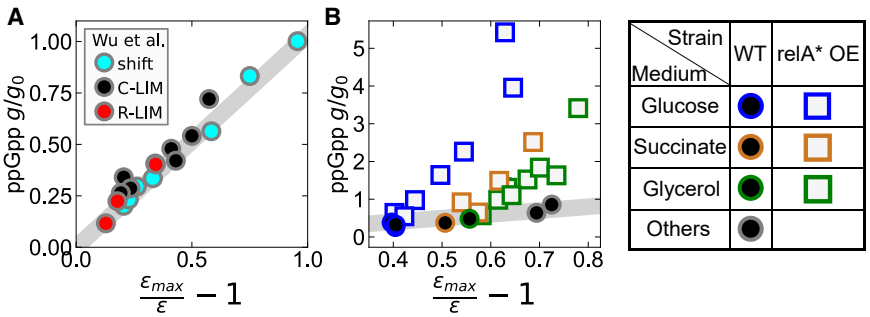

Figure 4. RelA* overexpression causes distorted sensing of elongation rates

(A) In the wild type, ppGpp levels are determined by the elongation rate ε via sensing by RelA, leading to Equation 11. Data from Wu et al.[20] for a diauxic shift (light blue), catabolic limitation (black), or chloramphenicol treatment (red).

(B) ppGpp levels versus elongation rates as calculated from our growth rate data, using the elongation rate growth law in Zhu and Dai.[37] Our estimates show that the linear wild-type relation in (A) does not hold under RelA* overexpression. At the same elongation rate ϵ, ppGpp is more abundant in RelA* overexpression mutants, reflecting the excess of synthase domains and the lack of compensation by SpoT.

For both (A) and (B), gray lines represent the best linear fit of wild-type data according to Equation 11, with $g_0 \approx 70\ pmol/OD_{600}$ for our data.

exclude the possibility of a DksA-limited regime, particularly for ppGpp values in the typical wild-type range, where branching is already recorded (Figure 3A). Indeed, existing observations report consistently high concentrations of DksA across various conditions.[18] Incidentally, the proteomics data from Mori et al.[9] report that the abundance of Crp, which is essential for cAMP signaling, increases under C-LIM in the wild type. This increase can be interpreted as an adaptation to cellular levels of cAMP, supporting frameworks such as ours,[33] in which cAMP functions as the sole regulator, without explicitly considering Crp. Refined models where a Crp-cAMP regulator is limited by Crp are possible, but these details appear to go beyond the question of transcriptional competition.

In principle, other scenarios can be conceived to describe our data. For instance, one might consider allowing ϕ_Q to vary, leading to various model configurations. We demonstrate that a model where the sector strength β_Q remains unchanged during RelA overexpression, while the P sector is treated as passive, fails to explain the observed data. This alternative model predicts a greater downregulation of the R sector compared with wild-type conditions, which contradicts our findings (Methods S1 for proof). As a second alternative, we explored a model where, under RelA overexpression, proteome resources released by the R sector are allocated to the Q sector, while ϕ_P remains constant. Within our framework, we demonstrate that cAMP-mediated activation of the P sector is still necessary in this scenario (Methods S1). Moreover, we note that while some catabolic and anabolic genes are upregulated by ppGpp,[19,66] considering this mechanism alone without activation by cAMP would predict ϕ_R to depend solely on ppGpp (Methods S1). Indeed, at equivalent ppGpp concentration, the P sector would be equally activated in RelA overexpression mutants and in the wild type, imposing the same degree of (indirect) repression on ϕ_R, contradicting the experimental findings in Figure 3A.

Thus, we conclude that, within the range of scenarios we considered, transcriptional competition is a necessary ingredient for the model to reproduce the behavior of our experimental data.

Suboptimal proteome allocation is maintained by distorted sensing of elongation rates

The observation that the $\phi_R - \lambda$ relationship is conserved under RelA overexpression, whereas the $\phi_R - g$ relationship is not, prompted us to investigate the behavior of other variables of the system with respect to ppGpp. Specifically, we focused on the relation between translation elongation rate ϵ and g. Wu and coworkers[20] reported a solid link in the wild type between these two variables, even under out-of-steady-state conditions (Figure 4A), as follows:

$$\frac{g}{g_0} = \frac{\varepsilon_{max}}{\varepsilon} - 1 \qquad \text{(Equation 11)}$$

where ε_{max} represents the maximal elongation rate, and g_0 denotes a reference ppGpp concentration. It has also been reported that the $\varepsilon - \phi_R$ (and hence $\varepsilon - \lambda$) relationship remains substantially unchanged under RelA* expression[37] (Figure S2); therefore, ppGpp overexpression cannot preserve the relationship established by Equation 11.

Figure 4B explicitly shows this point using the data in Zhu and Dai[37] to convert growth rates from our experiments into elongation rate values (STAR Methods) and plot them against ppGpp concentration. As expected, Figure 4B shows that RelA overexpression breaks Equation 11. In fact, at equivalent elongation rates, we find higher ppGpp concentrations in RelA* overexpression mutants. This change can be described as a distorted sensing of elongation rates by the cell.[20] At equivalent values of ϵ, cells perceive harsher conditions than those actually present. It is important to note that if the wild-type cAMP-ppGpp relation (Figure 2C) were conserved upon RelA* overexpression, our model would predict a collapse on the wild-type curve for ϕ_R as a function of ppGpp, despite distorted sensing of ϵ. Thus, distorted elongation rate sensing, combined with disrupted cAMP-ppGpp coordination, acts to maintain suboptimal proteome allocation when RelA is overexpressed.

We also note that this prediction is compatible with the theory proposed by Wu et al.[20] for the wild type. Here, the steady-state ppGpp concentration is given by the steady-state balance between synthesis by RelA, with rate a, and hydrolysis by SpoT, with first-order rate constant b, yielding $\frac{g^{eq}}{g_0} = \frac{a}{b}$. The synthesis rate is taken to be proportional to the number of "dwelling" ribosomes, and the hydrolysis rate to be proportional to the number of ribosomes in the translocating state of elongation, so that the ratio $\frac{a}{b}$ becomes a function of the elongation rate, $\frac{a}{b} = \frac{\varepsilon_{max}}{\varepsilon} - 1$, leading to Equation 11.

Assuming this theory, we can explain ppGpp overabundance in Figure 4 as follows. In the RelA overexpression strain, ppGpp is also synthesized by the truncated RelA enzyme, which has

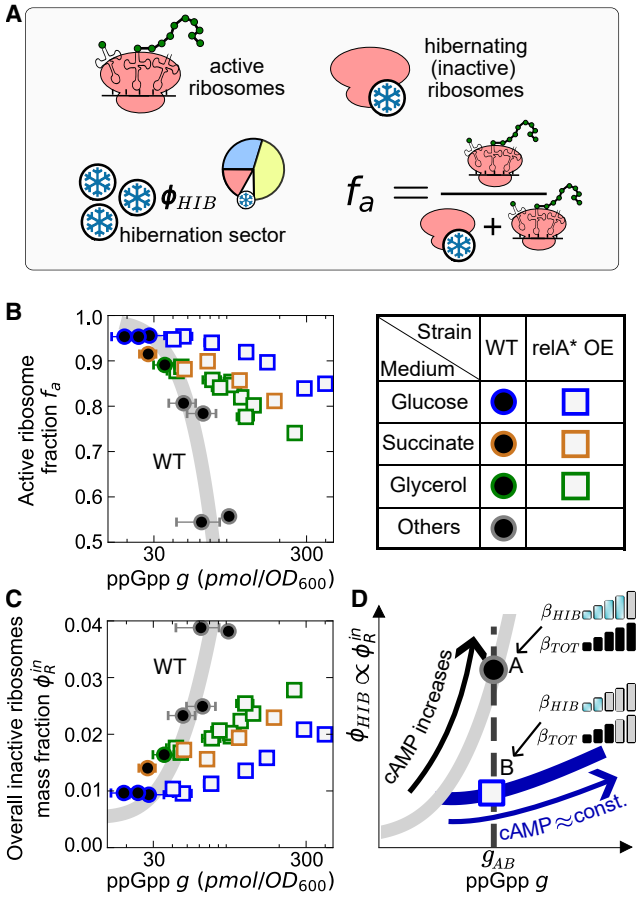

Figure 5. Transcriptional activation of hibernation factors by cAMP explains deviations in the fraction of active ribosomes

(A) Scheme of the model. We consider two populations of ribosomes: actively elongating ribosomes (with fraction f_a), which contribute to translation and growth, and hibernating (inactive) ribosomes. The proteome sector containing the hibernation factors has a mass fraction ϕ_{HIB}.

(B) Estimates for the fraction of active ribosomes $f_a := \frac{\lambda}{\epsilon\phi_R}$, calculated from our growth rate data, plotted against ppGpp. The gray line is obtained with this definition, using the wild-type growth laws for ϵ and ϕ_R as in Dai et al.[47] and Zhu and Dai[37] (see STAR Methods). Under RelA overexpression, f_a decreases as a function of ppGpp, but its decrease is less pronounced with respect to unperturbed data. Error bars represent standard error across technical replicates.

(C) Under RelA overexpression, the estimated proteome fraction corresponding to inactive ribosomes ϕ_R^{in} increases more gradually with ppGpp. The gray wild-type line is obtained analogously to the one in (A), through Equation 13 (STAR Methods).

(D) Results in (B) can be explained by a transcriptional competition theory in which hibernation factors are activated by both ppGpp and cAMP, with a strength β_{HIB}, explaining their scarcity under RelA overexpression.

constitutive activity.[41,67] We write ppGpp dynamics and its equilibrium concentration as follows:

$$\frac{d}{dt}\left(\frac{g}{g_0}\right) = a + k_* - b\frac{g}{g_0}$$
$$\frac{g^{eq}}{g_0} = \frac{a+k_*}{b} > \frac{\varepsilon_{max}}{\varepsilon} - 1 \qquad \text{(Equation 12)}$$

with the second equation representing the deviation in Figure 4B. Here k_* represents the constitutive synthase activity of RelA*, which varies with the degree of induction. Consistent with this, we compute k_* from our data and demonstrate its correlation with the concentration of the pTet inducer, doxycycline (Methods S1). As a result, for the same elongation rate ϵ (i.e., for the same number of dwelling and translocating ribosomes), RelA* induction corresponds to increased ppGpp.

We must also note that if we focus on a single carbon source, not only is ppGpp concentration higher than in the unperturbed condition, but ϵ also decreases ($\frac{\varepsilon_{max}}{\varepsilon} - 1$ increases). We attribute this change to the feedback loop between ppGpp and the translation apparatus.[36,46] We expect increasing ppGpp through RelA overexpression and keeping the nutrient source fixed to lead to transcriptional repression of tRNAs and translation factors, which are co-regulated with ribosomes. According to the theory by Dai et al.,[47] this would in turn cause ϵ to decrease.

Transcriptional regulation of hibernation factors explains deviations in ribosome inactivity

In addition to the elongation rate ϵ and ribosome proteome fraction ϕ_R, the fraction of actively translating ribosomes, f_a, is a crucial determinant of growth rate.[47] We can calculate f_a using the relationship $f_a = \frac{\lambda}{\epsilon\phi_R}$. This definition assumes negligible protein degradation, which plays a role in setting the fraction of active ribosomes, particularly at very low growth rates.[48] In the following, we maintain this simplifying assumption, as it provides a reasonable approximation in moderate-to-fast growth conditions.[36,48]

The main contribution to inactive ribosomes is generally attributed to ribosome deactivation by hibernation factors.[20] Other factors, such as stalled ribosomes[47] and mRNA scarcity,[29] might also play a role, but we focus for simplicity on inactivation by hibernation factors, following the model proposed in Wu et al.[20] In *E. coli*, four main hibernation factors, Rmf, RaiA, RsfS, and Hpf, dimerize or sequester ribosomes and their subunits,[68–70] thereby preventing them from initiating translation (Figure 5A). We group these factors into a new sector characterized by a mass fraction ϕ_{HIB} and assume complete binding of hibernation factors to ribosomes, expressed as

$$\phi_{HIB} \propto \phi_R^{in} = (1 - f_a)\phi_R, \qquad \text{(Equation 13)}$$

again in line with Wu et al.[20]. Here ϕ_R^{in} is the mass fraction associated with the inactive ribosomal sector.

Knowledge of λ and the values of ϕ_R and ϵ allows us to calculate f_a and ϕ_R^{in} in our data and plot them against ppGpp concentration (Figures 5B and 5C). Our results reveal a significant deviation from the wild-type relationship: at equivalent ppGpp concentrations, RelA overexpression mutants display higher values of the active fraction f_a, despite an overall decrease with overexpression. This suggests that ϕ_{HIB} is not regulated exclusively by ppGpp, as proposed in the model of Wu et al.[20]

We speculated that this fact might also be a consequence of transcriptional competition. To explore this possibility, we introduce a collective promoter strength associated with hibernation factors, β_{HIB}. Figure 5D provides a schematic representation of how second messengers could be influencing this variable in relation to the mass fraction ϕ_{HIB}, taking again glucose as a

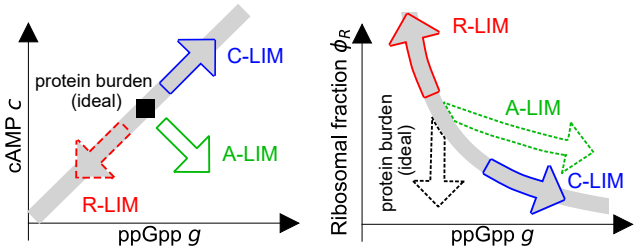

Figure 6. The C-LIM ppGpp-ribosome relationship can be preserved or broken under different perturbations

In our framework, different perturbations can be visualized as displacements in the ppGpp-cAMP plane. Following the C-LIM curve in this plane (gray line, left) is both necessary and sufficient for a perturbation to preserve the C-LIM ppGpp-ribosome relationship (gray line, right), due to Equation 9. This principle allows us to make predictions (dashed arrows) for untested perturbations based on relationships inferred from existing literature measurements (solid arrows). Under anabolic limitation (A-LIM, green), assuming that ppGpp and cAMP anticorrelate[40] leads to a divergence in the ppGpp-ribosome plane. We predict ppGpp and cAMP should covary under chloramphenicol treatment (R-LIM, red), as literature data[20,47] suggest the ppGpp-ribosome relationship should be conserved. Expression of a useless protein (black) can ideally lead to a decrease in ribosome content without any change in ppGpp, due to RNAP diversion.

reference. At the same ppGpp concentration g_{AB}, the wild type (point A) presents a higher cAMP concentration than the RelA overexpression mutant (point B), i.e., $c_A > c_B$. Our data indicate that $\phi_{HIB}(B) > \phi_{HIB}(A)$, which at steady-state can be written in terms of promoter strengths from Equation 7 (see STAR Methods for derivation):

$$\frac{\beta_{HIB}(A)}{\beta_R(g_{AB}) + \beta_P(c_A)}\phi_{max} > \frac{\beta_{HIB}(B)}{\beta_R(g_{AB}) + \beta_P(c_B)}\phi_{max} \qquad \text{(Equation 14)}$$

This inequality captures the competition between the hibernation sector in the numerators and the P and R sectors in the denominators. Since the denominator is greater for the wild type (left-hand side) due to the activation of the P sector by cAMP, the inequality suggests that the strength of the hibernation sector must also be higher in wild-type cells, i.e., $\beta_{HIB}(A) > \beta_{HIB}(B)$.

This model shows that the data are consistent with cAMP activating the hibernation sector, in addition to the reported effect by ppGpp.[20] Notably, here the deviation from the wild-type line arises from a direct regulatory effect, rather than simply from competition for RNAP, as was observed for the ribosomal fraction ϕ_R (Figure 3C). Indeed, global coupling acts on the denominator, and taken alone, it would cause the opposite relationship: $\phi_{HIB}(A) < \phi_{HIB}(B)$ due to activation of the P sector by cAMP, with $\beta_P(c_A) > \beta_P(c_B)$. Therefore, we hypothesize that cAMP may regulate a direct transcriptional activation of the hibernation sector. In line with this claim, cAMP was found to activate transcription of *rmf* and *raiA*.[70,71]

This transcriptional model for hibernation factors may also explain why the ribosomal growth law $\phi_R(\lambda)$ remains the same as the wild type under anabolic limitation (A-LIM)[33,40] and in the "cAMP titration" strain examined in Kochanowski et al.[40] Its conservation suggests that both ϵ and f_a must are able to adjust to ribosomal abundance across these perturbations, which we predict to break the ppGpp-cAMP relationship seen under C-LIM (see below).

The model predicts ppGpp-ribosome divergence under alternative perturbations

In addition to RelA overexpression, there may be other situations in which competition between regulons determines a deviation from the ppGpp-ribosome relationship observed under C-LIM. An important example is titration of the enzyme glutamate synthase,[40] which imposes an A-LIM. In this condition, cAMP levels decrease as growth rate declines, and ribosome abundance falls according to the same growth law observed under C-LIM.[33,40] The catabolic sector also decreases, which can be attributed to regulation by cAMP. However, indirect effects of cAMP alone would be expected to increase the ribosomal fraction through transcriptional competition. Therefore, the observed reduction in ribosomes must reflect direct repression by elevated ppGpp.[1] Thus, in the light of our model, these findings support the interpretation that ppGpp and cAMP should be anticorrelated under A-LIM.[40] In other words, if this perturbation originates from a point on the C-LIM curve, the system should move into the region of the ppGpp-cAMP plane below that curve (Figure 6, solid green arrow). Based on this interpretation, we predict indirect cAMP effects will create an apparent weakening of ppGpp's repressive power (Methods S1), similar to what we observed under RelA overexpression (Figure 3). Thus, transcriptional competition effects should be detectable as a divergence from the C-LIM relationship between ppGpp and ϕ_R, as indicated by the dashed green arrow in Figure 6.

Another situation in which competition could emerge is growth inhibition by antibiotics such as chloramphenicol (R-LIM), which leads to ppGpp depletion, opposite to RelA overexpression.[6,9,47] These two perturbations are fundamentally different in that R-LIM leaves the feedback loop between ppGpp and translation machinery intact. Indeed, it appears to preserve the key regulatory relationship between ppGpp and elongation rate[20] (Figure 4A), as well as the one between elongation rate and ribosomal sector ϕ_R[47] (Figure S4). Given these conserved links, we conclude that the ppGpp-ϕ_R relationship should also be conserved, as shown by the solid red arrow in Figure 6 (Methods S1). While paired ppGpp-cAMP measurements are not available under this condition, the ppGpp-ϕ_R conservation emerges in the model if cAMP and ppGpp covary (dashed red arrow in Figure 6). Consistent with this inference, R-LIM has been reported to interfere with cAMP signaling[72,73]; however, it also induces distortions that require careful consideration (see discussion).

Lastly, we consider a perturbation by the overexpression of a useless protein.[6,33] Here, the details of ppGpp regulation (e.g., whether the $\varepsilon - g$ relationship in Figure 4A is maintained) remain incompletely understood, and no joint ppGpp-cAMP measurements are available. Therefore, we examine an idealized scenario in which overexpression does not alter ppGpp or cAMP levels. Even in the absence of such changes, allocation of RNAP to express the useless gene can decrease the ribosomal fraction (dashed black arrow in Figure 6) via transcriptional competition (Methods S1). Thus, we predict that, in this simplified scenario, transcriptional competition should manifest again as a splitting in the ribosome-ppGpp relationship from the C-LIM line.

DISCUSSION

While there is a large body of work on how different regulators control the various components of the proteome,[20,33,40,57] the

impact of these regulatory circuits on the global scale is relatively unexplored.[1,31,40,74–76] In *Escherichia coli*, the prevailing consensus sees ppGpp alone as a governor of ribosome allocation, overriding the influence of other regulators.[16,40] However, data collected in this study confirm the previous observation[41,42,44] that ribosome allocation is not solely dependent on ppGpp outside physiological conditions. Indeed, ppGpp's capacity to repress expression of ribosomes is decreased under RelA overexpression (Figure 3A).

The primary result of our combined approach, integrating coarse-grained modeling and data, is that allocation of RNAP toward catabolic genes decreases expression of ribosomal genes. This is a form of indirect repression that requires no direct regulatory interactions between Crp and cAMP with ribosomal promoters. Instead, cAMP acts by inducing the expression of catabolic genes, which compete for RNAP allocation with ribosomal protein genes (Figure 3C). RelA overexpression was required to reveal this competition, which is otherwise obscured in the wild type by the approximately linear relationship between cAMP and ppGpp (Figure 2C).

This relationship, observed under C-LIM, is consistent with theoretical predictions by Erickson et al.[53] and Scott and Hwa.[1] They propose that the correlation between ppGpp and cAMP arises from a mechanistic link between the two messengers, possibly due to their sensitivity to ketoacids and amino acids, which are coupled via transamination. Under this framework, the disruption of the correlation under RelA overexpression could be attributed to ppGpp's distorted sensing of the elongation rate and, consequently, of the amino acid pool. Alternatively, the correlation might be non-causal, simply reflecting the shared role of ppGpp and cAMP as stress signals under C-LIM. Whether this relationship is causal remains an open question for future investigation.

Our theory places cAMP on par with ppGpp as "orthogonal" signals: not only do they control different parts of the proteome, but their levels must also be independently adjusted, since we observed deviations from the wild-type ppGpp-cAMP curve under RelA overexpression (Figure 3B). However, some interactions have been reported, ranging from ppGpp-induced acetylation of Crp[77] and direct binding of ppGpp to Crp, which can impair its activity.[62,78] These non-orthogonal effects can be included in the ρ factor in Equation 10, without substantial changes to the model (Methods S1).

The anabolic (A) sector plays a key role in the interplay between ppGpp and cAMP, as it links catabolism to ribosomes.[1,33] In our work, we approximated it as constitutive (passively regulated), following the approach of Kochanowski and coworkers.[40] In line with their conclusion, we emphasize that this is only an approximation, and pathway-specific regulators may dominate the control of this sector. Indeed, downregulation of the A sector under C-LIM,[9,33] as observed experimentally, is inconsistent with constitutive-like behavior, since expression from constitutive promoters is expected to increase in this condition.[31] To demonstrate that our model remains valid regardless of this approximation, we have attempted a more data-driven approach in defining the sector that competes with ribosomes, using gene targets of cAMP as cataloged in databases such as RegulonDB[58] and EcoCyc[59] (consulted February 2025), rather than relying on phenomenological definitions of proteome sectors. Our analysis revealed that cAMP-activated genes are distributed across the entire proteome, including the Q sector (Figures S5A and S5B). As a result, ribosomal proteins may be considered in competition for RNAP with a "cAMP-activated sector" that does not perfectly overlap with catabolic proteins. This variant adequately describes the data, requiring only a modification of parameters (Table S1 and Methods S1).

One important additional layer of regulation, particularly under conditions of high ppGpp, is the contribution of alternative sigma factors,[79] which can be naturally incorporated into our model (see Methods S1 for mathematical details). Alternative-sigma-factor-induced genes can compete with RpoD-dependent genes in several ways. First, as classically noted, they may compete for core RNAP (the well-known sigma factor competition[79,80]), a scenario that is unlikely to be quantitatively relevant in moderate-to-fast-growing wild type, given that core RNAP is typically in excess and maintained at a constant level.[31] Second, mRNAs expressed from alternative sigmulons can reduce the fraction of the transcriptome corresponding to RpoD-dependent genes, thereby decreasing their protein mass fraction, without affecting their total mRNA abundance. This effect can be captured by the model in the main text (Equation 7), simply by introducing a sector corresponding to the alternative sigmulon (Methods S1).

Although alternative sigma factors may respond to second messengers,[79,81] their quantitative cross-talk remains unclear. In principle, they could become relevant under extreme ppGpp overabundance, where cellular adaptations to growth slowdowns, which fall outside the scope of this study, could influence the system. However, recent data by Zhu et al.[39] show that, although RelA overexpression in glucose upregulates RpoS-dependent genes, the overall response remains largely unaltered in an *rpoS* knockout. Furthermore, our proteomic analysis of the sigma factor landscape under RelA overexpression (based on data from Zhu and Dai.[38] and Zhu et al.[39]) indicates that the other sigma factors remain substantially unresponsive, and core RNAP is maintained in excess (Figure S6), despite a fivefold increase in ppGpp. Analysis of the same dataset revealed that RelA overexpression activates cAMP-responsive genes (Figure S5B), consistent with predictions from our model via indirect effects (Figure 3C). Overall, these observations indicate that alternative sigma factors do not strongly affect the system under the conditions examined; nonetheless, their interplay with global transcriptional programs remains to be explored.

Our model can be applied to predict responses for perturbations beyond RelA overexpression (Figure 6). We predict that, under A-LIM, the negative correlation between cAMP and ppGpp should cause a divergence from the C-LIM ppGpp-ϕ_R relationship. In future studies, joint measurements of ppGpp and ribosome abundance under A-LIM could provide further model validation and allow quantification of transcriptional competition in this condition. Conversely, based on literature data and our model, we infer that R-LIM should preserve the cAMP-ppGpp covariance. We note, however, that R-LIM can induce polarity effects due to premature transcriptional termination in ribosomal protein operons, causing a progressive decrease in mRNA abundance along the operon.[37] As a result, the assumption of a single "coarse-grained" initiation rate for all ribosomal genes may be compromised, as ribosomal mRNA production becomes non-stoichiometric. Therefore, testing the

model under R-LIM would require not only measuring growth rate or ribosome abundance but also accounting for the distortive effects introduced by polarity.

The remarkably robust conservation of the ribosomal growth law $\phi_R(\lambda)$ under both ppGpp and cAMP titration[37,40] in the absence of coupling between the two messengers requires an explanation. To maintain consistency, we showed that the fraction of active ribosomes f_a must not depend solely on ppGpp. Our analysis shows that a theory of transcriptional regulation of ribosome-hibernating factors can capture this behavior. Specifically, we speculate that activation of the hibernation sector by cAMP could be one of the factors contributing to this observation, thereby recreating the growth law. While there is evidence of a role of cAMP in regulating this sector,[70,71] additional studies on this point are required, as hibernation factors could also be regulated post-transcriptionally (raiA and rmf in Melamed et al.[82]), or additional mechanisms might influence their binding to ribosomes.[70]

More widely, our findings show how the global effects of gene transcription should be understood within a framework of RNAP allocation,[30,31,83] similar to the established proteome allocation model. Rather than viewing ppGpp as a direct regulator of ribosomal content, we show that its effects arise through global RNAP redistribution, influenced by competition with other transcriptional programs. This perspective clarifies why changes in ppGpp levels alone do not fully predict ribosome synthesis and why conditions, such as ppGpp overabundance, alter proteome composition in ways not captured by traditional promoter-centric models. Although second-messenger signaling varies across organisms (for example, catabolite repression and ppGpp function differently in other bacteria[84–86]), our framework provides a generalizable approach for understanding global competition effects in transcriptional regulation. As a result, we believe that the principles and consequences of competition described in this study may play a general role in cellular responses across different species.

RESOURCE AVAILABILITY

Lead contact

Requests for further information and resources should be directed to and will be fulfilled by the lead contact, Marco Cosentino Lagomarsino (marco.cosentino-lagomarsino@ifom.eu).

Materials availability

This study did not generate new materials.

Data and code availability

- Data associated with this work have been deposited in Zenodo and are publicly available as of the date of publication at 10.5281/zenodo.18097448.
- All original code has been deposited in Zenodo and is publicly available as of the date of publication at 10.5281/zenodo.18097448.
- Any additional information required to reanalyze the data reported in this paper is available from the lead contact upon request.

ACKNOWLEDGMENTS

We thank Gabriele Micali, Luca Ciandrini, Bianca Sclavi, Philippe Fuchs, Martina Dal Bello, and Paul Wiggins for useful discussions on this work. We thank Ferhat Büke, Marek Noga, Flora Yang, and Adja Zoumaro-Djayoon for technical assistance with ppGpp and cAMP quantification. The research leading to these results has received funding from AIRC under IG 2024-ID 30391 project (to M.C.L.). R.D. was supported by the AIRC fellowship, Italy Pre-Doc 2022 (ID 28176). G.B. is supported by the Netherlands Organization for Scientific Research (NWO). M.L. was supported as part of the Frontiers of Nanoscience program.

AUTHOR CONTRIBUTIONS

Conceptualization, G.B. and M.C.L.; theoretical investigation, A.R. and R.D.; experiments, M.L.; data analysis, A.R., M.L., and R.D; writing, A.R. and M.C.L.; funding acquisition, M.C.L., G.B., and R.D.; supervision, M.C.L. and G.B.

DECLARATION OF INTERESTS

The authors declare no competing interests.

DECLARATION OF GENERATIVE AI AND AI-ASSISTED TECHNOLOGIES IN THE WRITING PROCESS

During the preparation of this work, the authors used ChatGPT for minor rephrasing of the text. After using this tool, the authors reviewed and edited the content as needed and take full responsibility for the content of the publication.

STAR★METHODS

Detailed methods are provided in the online version of this paper and include the following:

- KEY RESOURCES TABLE
- EXPERIMENTAL MODEL DETAILS
  - Strains and plasmids
  - Culture conditions
- METHOD DETAILS
  - Sample collection and analysis for ppGpp and cAMP quantification
  - Growth rate measurements
  - ppGpp and cAMP quantification via LC/MS
- QUANTIFICATION AND STATISTICAL ANALYSIS
  - Conversion of growth rates into ribosomal fractions and elongation rates
  - Generating the wild-type active ribosomes-ppGpp curve (Figure 5)
  - Modeling – coarse grained promoter strengths
  - Modeling – gene dosage effects
  - Fitting the model of transcriptional competition to ribosomal fractions
  - Transcriptional competition theory for hibernation factors
  - Definition of regulatory sectors for model–proteomics comparison

SUPPLEMENTAL INFORMATION

Supplemental information can be found online at https://doi.org/10.1016/j.cels.2026.101609.

Received: April 15, 2025
Revised: December 21, 2025
Accepted: April 15, 2026
Published: May 13, 2026

REFERENCES

1. Scott, M., and Hwa, T. (2023). Shaping bacterial gene expression by physiological and proteome allocation constraints. Nat. Rev. Microbiol. *21*, 327–342. https://doi.org/10.1038/s41579-022-00818-6.
2. López-Maury, L., Marguerat, S., and Bähler, J. (2008). Tuning gene expression to changing environments: from rapid responses to

evolutionary adaptation. Nat. Rev. Genet. *9*, 583–593. https://doi.org/10.1038/nrg2398.

3. Lee, T.I., and Young, R.A. (2013). Transcriptional regulation and its misregulation in disease. Cell *152*, 1237–1251. https://doi.org/10.1016/j.cell.2013.02.014.
4. Lo, T.W., Choi, H.J., Huang, D., and Wiggins, P.A. (2024). Noise robustness and metabolic load determine the principles of central dogma regulation. Sci. Adv. *10*, eado3095. https://doi.org/10.1126/sciadv.ado3095.
5. Hofmeyr, J.S., and Cornish-Bowden, A. (2000). Regulating the cellular economy of supply and demand. FEBS Lett. *476*, 47–51. https://doi.org/10.1016/S0014-5793(00)01668-9.
6. Scott, M., Gunderson, C.W., Mateescu, E.M., Zhang, Z., and Hwa, T. (2010). Interdependence of cell growth and gene expression: Origins and consequences. Science *330*, 1099–1102. https://doi.org/10.1126/science.1192588.
7. Scott, M., Klumpp, S., Mateescu, E.M., and Hwa, T. (2014). Emergence of robust growth laws from optimal regulation of ribosome synthesis. Mol. Syst. Biol. *10*, 747. https://doi.org/10.15252/msb.20145379.
8. Hui, S., Silverman, J.M., Chen, S.S., Erickson, D.W., Basan, M., Wang, J., Hwa, T., and Williamson, J.R. (2015). Quantitative proteomic analysis reveals a simple strategy of global resource allocation in bacteria. Mol. Syst. Biol. *11*, 784. https://doi.org/10.15252/msb.20145697.
9. Mori, M., Zhang, Z., Banaei-Esfahani, A., Lalanne, J.B., Okano, H., Collins, B.C., Schmidt, A., Schubert, O.T., Lee, D.S., Li, G.W., et al. (2021). From coarse to fine: the absolute escherichia coli proteome under diverse growth conditions. Mol. Syst. Biol. *17*, e9536. https://doi.org/10.15252/msb.20209536.
10. Zhu, M., and Dai, X. (2024). Shaping of microbial phenotypes by trade-offs. Nat. Commun. *15*, 4238. https://doi.org/10.1038/s41467-024-48591-9.
11. Neidhardt, F.C., and Magasanik, B. (1960). Studies on the role of ribonucleic acid in the growth of bacteria. Biochim. Biophys. Acta *42*, 99–116. https://doi.org/10.1016/0006-3002(60)90757-5.
12. Aebersold, R., and Mann, M. (2016). Mass-spectrometric exploration of proteome structure and function. Nature *537*, 347–355. https://doi.org/10.1038/nature19949.
13. Beck, M., Schmidt, A., Malmstroem, J., Claassen, M., Ori, A., Szymborska, A., Herzog, F., Rinner, O., Ellenberg, J., and Aebersold, R. (2011). The quantitative proteome of a human cell line. Mol. Syst. Biol. *7*, 549. https://doi.org/10.1038/msb.2011.82.
14. Metzl-Raz, E., Kafri, M., Yaakov, G., Soifer, I., Gurvich, Y., and Barkai, N. (2017). Principles of cellular resource allocation revealed by condition-dependent proteome profiling. eLife *6*, e28034. https://doi.org/10.7554/eLife.28034.
15. Zhu, M., Mori, M., Hwa, T., and Dai, X. (2025). Distantly related bacteria share a rigid proteome allocation strategy with flexible enzyme kinetics. Proc. Natl. Acad. Sci. USA *122*, e2427091122. https://doi.org/10.1073/pnas.2427091122.
16. Potrykus, K., Murphy, H., Philippe, N., and Cashel, M. (2011). ppgpp is the major source of growth rate control in E. coli. Environ. Microbiol. *13*, 563–575. https://doi.org/10.1111/j.1462-2920.2010.02357.x.
17. Barker, M.M., Gaal, T., Josaitis, C.A., and Gourse, R.L. (2001). Mechanism of regulation of transcription initiation by ppgpp. I. effects of ppgpp on transcription initiation in vivo and in vitro. J. Mol. Biol. *305*, 673–688. https://doi.org/10.1006/jmbi.2000.4327.
18. Lemke, J.J., Sanchez-Vazquez, P., Burgos, H.L., Hedberg, G., Ross, W., and Gourse, R.L. (2011). Direct regulation of escherichia coli ribosomal protein promoters by the transcription factors ppgpp and dksa. Proc. Natl. Acad. Sci. USA *108*, 5712–5717. https://doi.org/10.1073/pnas.1019383108.
19. Sanchez-Vazquez, P., Dewey, C.N., Kitten, N., Ross, W., and Gourse, R.L. (2019). Genome-wide effects on Escherichia coli transcription from ppgpp binding to its two sites on rna polymerase. Proc. Natl. Acad. Sci. USA *116*, 8310–8319. https://doi.org/10.1073/pnas.1819682116.
20. Wu, C., Balakrishnan, R., Braniff, N., Mori, M., Manzanarez, G., Zhang, Z., and Hwa, T. (2022). Cellular perception of growth rate and the mechanistic origin of bacterial growth law. Proc. Natl. Acad. Sci. USA *119*, e2201585119. https://doi.org/10.1073/pnas.2201585119.
21. Irving, S.E., Choudhury, N.R., and Corrigan, R.M. (2021). The stringent response and physiological roles of (pp)pgpp in bacteria. Nat. Rev. Microbiol. *19*, 256–271. https://doi.org/10.1038/s41579-020-00470-y.
22. Loveland, A.B., Bah, E., Madireddy, R., Zhang, Y., Brilot, A.F., Grigorieff, N., and Korostelev, A.A. (2016). Ribosome·RelA structures reveal the mechanism of stringent response activation. eLife *5*, e17029. https://doi.org/10.7554/eLife.17029.
23. Arenz, S., Abdelshahid, M., Sohmen, D., Payoe, R., Starosta, A.L., Berninghausen, O., Hauryliuk, V., Beckmann, R., and Wilson, D.N. (2016). The stringent factor RelA adopts an open conformation on the ribosome to stimulate ppgpp synthesis. Nucleic Acids Res. *44*, 6471–6481. https://doi.org/10.1093/nar/gkw470.
24. Potrykus, K., and Cashel, M. (2008). (p)ppgpp: still magical? Annu. Rev. Microbiol. *62*, 35–51. https://doi.org/10.1146/annurev.micro.62.081307.162903.
25. Zhu, M., Pan, Y., and Dai, X. (2019). (p)ppgpp: the magic governor of bacterial growth economy. Curr. Genet. *65*, 1121–1125. https://doi.org/10.1007/s00294-019-00973-z.
26. Mu, H., Han, F., Wang, Q., Wang, Y., Dai, X., and Zhu, M. (2023). Recent functional insights into the magic role of (p)ppgpp in growth control. Comput. Struct. Biotechnol. J. *21*, 168–175. https://doi.org/10.1016/j.csbj.2022.11.063.
27. Lin, J., and Amir, A. (2018). Homeostasis of protein and mRNA concentrations in growing cells. Nat. Commun. *9*, 4496. https://doi.org/10.1038/s41467-018-06714-z.
28. Roy, A., Goberman, D., and Pugatch, R. (2021). A unifying autocatalytic network-based framework for bacterial growth laws. Proc. Natl. Acad. Sci. USA *118*, e2107829118. https://doi.org/10.1073/pnas.2107829118.
29. Calabrese, L., Ciandrini, L., and Cosentino Lagomarsino, M. (2024). How total mrna influences cell growth. Proc. Natl. Acad. Sci. USA *121*, e2400679121. https://doi.org/10.1073/pnas.2400679121.
30. Klumpp, S., Zhang, Z., and Hwa, T. (2009). Growth rate-dependent global effects on gene expression in bacteria. Cell *139*, 1366–1375. https://doi.org/10.1016/j.cell.2009.12.001.
31. Balakrishnan, R., Mori, M., Segota, I., Zhang, Z., Aebersold, R., Ludwig, C., and Hwa, T. (2022). Principles of gene regulation quantitatively connect dna to rna and proteins in bacteria. Science *378*, eabk2066. https://doi.org/10.1126/science.abk2066.
32. Fic, E., Bonarek, P., Gorecki, A., Kedracka-Krok, S., Mikolajczak, J., Polit, A., Tworzydlo, M., Dziedzicka-Wasylewska, M., and Wasylewski, Z. (2008). cAMP Receptor Protein from Escherichia coli as a Model of Signal Transduction in Proteins – A Review. J. Mol. Microbiol. Biotechnol. *17*, 1–11. https://doi.org/10.1159/000178014.
33. You, C., Okano, H., Hui, S., Zhang, Z., Kim, M., Gunderson, C.W., Wang, Y.P., Lenz, P., Yan, D., and Hwa, T. (2013). Coordination of bacterial proteome with metabolism by cyclic AMP signalling. Nature *500*, 301–306. https://doi.org/10.1038/nature12446.
34. Fung, D.K., Trinquier, A.E., and Wang, J.D. (2023). Crosstalk between (p)ppgpp and other nucleotide second messengers. Curr. Opin. Microbiol. *76*, 102398. https://doi.org/10.1016/j.mib.2023.102398.
35. Towbin, B.D., Korem, Y., Bren, A., Doron, S., Sorek, R., and Alon, U. (2017). Optimality and sub-optimality in a bacterial growth law. Nat. Commun. *8*, 14123. https://doi.org/10.1038/ncomms14123.
36. Droghetti, R., Fuchs, P., Iuliani, I., Firmano, V., Tallarico, G., Calabrese, L., Grilli, J., Sclavi, B., Ciandrini, L., and Cosentino Lagomarsino, M. (2025). Incoherent feedback from coupled amino acids and ribosome pools generates damped oscillations in growing E. coli. Nat. Commun. *16*, 3063. https://doi.org/10.1038/s41467-025-57789-4.

37. Zhu, M., and Dai, X. (2019). Growth suppression by altered (p)ppgpp levels results from non-optimal resource allocation in escherichia coli. Nucleic Acids Res. *47*, 4684–4693. https://doi.org/10.1093/nar/gkz211.

38. Zhu, M., and Dai, X. (2023). Stringent response ensures the timely adaptation of bacterial growth to nutrient downshift. Nat. Commun. *14*, 467. https://doi.org/10.1038/s41467-023-36254-0.

39. Zhu, M., Mu, H., and Dai, X. (2024). Integrated control of bacterial growth and stress response by (p)ppgpp in Escherichia coli: A seesaw fashion. iScience *27*, 108818. https://doi.org/10.1016/j.isci.2024.108818.

40. Kochanowski, K., Okano, H., Patsalo, V., Williamson, J., Sauer, U., and Hwa, T. (2021). Global coordination of metabolic pathways in escherichia coli by active and passive regulation. Mol. Syst. Biol. *17*, e10064. https://doi.org/10.15252/msb.202010064.

41. Schreiber, G., Metzger, S., Aizenman, E., Roza, S., Cashel, M., and Glaser, G. (1991). Overexpression of the rela gene in Escherichia coli. J. Biol. Chem. *266*, 3760–3767. https://doi.org/10.1016/S0021-9258(19)67860-9.

42. Noga, M.J., Büke, F., van den Broek, N.J.F., Imholz, N.C.E., Scherer, N., Yang, F., and Bokinsky, G. (2020). Posttranslational control of plsb is sufficient to coordinate membrane synthesis with growth in escherichia coli. mBio *11*, e02703-19. https://doi.org/10.1128/mbio.02703-19.

43. Spira, B., and Ospino, K. (2020). Diversity in E. coli (p)ppgpp levels and its consequences. Front. Microbiol. *11*, 1759. https://doi.org/10.3389/fmicb.2020.01759.

44. Imholz, N.C.E., Noga, M.J., van den Broek, N.J.F., and Bokinsky, G. (2020). Calibrating the bacterial growth rate speedometer: A re-evaluation of the relationship between basal ppgpp, growth, and rna synthesis in escherichia coli. Front. Microbiol. *11*, 574872. https://doi.org/10.3389/fmicb.2020.574872.

45. Bosdriesz, E., Molenaar, D., Teusink, B., and Bruggeman, F.J. (2015). How fast-growing bacteria robustly tune their ribosome concentration to approximate growth-rate maximization. FEBS Journal *282*, 2029–2044. https://doi.org/10.1111/febs.13258.

46. Chure, G., and Cremer, J. (2023). An optimal regulation of fluxes dictates microbial growth in and out of steady state. eLife *12*, e84878. https://doi.org/10.7554/eLife.84878.

47. Dai, X., Zhu, M., Warren, M., Balakrishnan, R., Patsalo, V., Okano, H., Williamson, J.R., Fredrick, K., Wang, Y.P., and Hwa, T. (2016). Reduction of translating ribosomes enables *Escherichia coli* to maintain elongation rates during slow growth. Nat. Microbiol. *2*, 16231. https://doi.org/10.1038/nmicrobiol.2016.231.

48. Calabrese, L., Grilli, J., Osella, M., Kempes, C.P., Lagomarsino, M.C., and Ciandrini, L. (2022). Protein degradation sets the fraction of active ribosomes at vanishing growth. PLOS Comput. Biol. *18*, e1010059. https://doi.org/10.1371/journal.pcbi.1010059.

49. Zhu, M., and Dai, X. (2025). Systematic modulation of bacterial resource allocation by perturbing rna polymerase availability via synthetic transcriptional switches. Nucleic Acids Res. *53*, gkaf814. https://doi.org/10.1093/nar/gkaf814.

50. Klumpp, S., and Hwa, T. (2014). Bacterial growth: global effects on gene expression, growth feedback and proteome partition. Curr. Opin. Biotechnol. *28*, 96–102. https://doi.org/10.1016/j.copbio.2014.01.001.

51. Hauryliuk, V., Atkinson, G.C., Murakami, K.S., Tenson, T., and Gerdes, K. (2015). Recent functional insights into the role of (p)ppgpp in bacterial physiology. Nat. Rev. Microbiol. *13*, 298–309. https://doi.org/10.1038/nrmicro3448.

52. Zhu, M., Mori, M., Hwa, T., and Dai, X. (2019). Disruption of transcription-translation coordination in escherichia coli leads to premature transcriptional termination. Nat. Microbiol. *4*, 2347–2356. https://doi.org/10.1038/s41564-019-0543-1.

53. Erickson, D.W., Schink, S.J., Patsalo, V., Williamson, J.R., Gerland, U., and Hwa, T. (2017). A global resource allocation strategy governs growth transition kinetics of escherichia coli. Nature *551*, 119–123. https://doi.org/10.1038/nature24299.

54. Okano, H., Hermsen, R., Kochanowski, K., and Hwa, T. (2020). Regulation underlying hierarchical and simultaneous utilization of carbon substrates by flux sensors in escherichia coli. Nat. Microbiol. *5*, 206–215. https://doi.org/10.1038/s41564-019-0610-7.

55. Wehrens, M., Krah, L.H.J., Towbin, B.D., Hermsen, R., and Tans, S.J. (2023). The interplay between metabolic stochasticity and camp-crp regulation in single *E. coli* cells. Cell Rep. *42*, 113284. https://doi.org/10.1016/j.celrep.2023.113284.

56. Botsford, J.L., and Harman, J.G. (1992). Cyclic amp in prokaryotes. Microbiol. Rev. *56*, 100–122. https://doi.org/10.1128/mr.56.1.100-122.1992.

57. Kochanowski, K., Gerosa, L., Brunner, S.F., Christodoulou, D., Nikolaev, Y.V., and Sauer, U. (2017). Few regulatory metabolites coordinate expression of central metabolic genes in escherichia coli. Mol. Syst. Biol. *13*, 903. https://doi.org/10.15252/msb.20167402.

58. Salgado, H., Gama-Castro, S., Lara, P., Mejia-Almonte, C., Alarcón-Carranza, G., López-Almazo, A.G., Betancourt-Figueroa, F., Peña-Loredo, P., Alquicira-Hernández, S., Ledezma-Tejeida, D., et al. (2024). Regulondb v12.0: a comprehensive resource of transcriptional regulation in E. coli k-12. Nucleic Acids Res. *52*, D255–D264. https://doi.org/10.1093/nar/gkad1072.

59. Moore, L.R., Caspi, R., Boyd, D., Berkmen, M., Mackie, A., Paley, S., and Karp, P.D. (2024). Revisiting the y-ome of escherichia coli. Nucleic Acids Res. *52*, 12201–12207. https://doi.org/10.1093/nar/gkae857.

60. Droghetti, R., Corigliano, M., Calabrese, L., Fuchs, P., Vaidyanathan, A., Keisers, J., Micali, G., Lagomarsino, M.C., and Ciandrini, L. (2025). The hands-on growth laws theory cookbook. Preprint at arXiv. https://doi.org/10.48550/arXiv.2507.19194.

61. Büke, F., Grilli, J., Cosentino Lagomarsino, M., Bokinsky, G., and Tans, S.J. (2022). ppgpp is a bacterial cell size regulator. Curr. Biol. *32*, 870–877.e5. https://doi.org/10.1016/j.cub.2021.12.033.

62. Duysak, T., Tran, T.T., Afzal, A.R., and Jung, C.H. (2021). Fluorescence spectroscopic analysis of ppgpp binding to camp receptor protein and histone-like nucleoid structuring protein. Int. J. Mol. Sci. *22*, 7871. https://doi.org/10.3390/ijms22157871.

63. Fernández-Coll, L., Maciag-Dorszynska, M., Tailor, K., Vadia, S., Levin, P.A., Szalewska-Palasz, A., and Cashel, M. (2020). The absence of (p)ppgpp renders initiation of escherichia coli chromosomal dna synthesis independent of growth rates. mBio *11*, e03223-19. https://doi.org/10.1128/mBio.03223-19.

64. Paul, B.J., Barker, M.M., Ross, W., Schneider, D.A., Webb, C., Foster, J.W., and Gourse, R.L. (2004). Dksa: A critical component of the transcription initiation machinery that potentiates the regulation of rrna promoters by ppgpp and the initiating ntp. Cell *118*, 311–322. https://doi.org/10.1016/j.cell.2004.07.009.

65. Chandrangsu, P., Lemke, J.J., and Gourse, R.L. (2011). The dksa promoter is negatively feedback regulated by dksa and ppgpp. Mol. Microbiol. *80*, 1337–1348. https://doi.org/10.1111/j.1365-2958.2011.07649.x.

66. Paul, B.J., Berkmen, M.B., and Gourse, R.L. (2005). Dksa potentiates direct activation of amino acid promoters by ppgpp. Proc. Natl. Acad. Sci. USA *102*, 7823–7828. https://doi.org/10.1073/pnas.0501170102.

67. Svitil, A.L., Cashel, M., and Zyskind, J.W. (1993). Guanosine tetraphosphate inhibits protein synthesis in vivo. a possible protective mechanism for starvation stress in *Escherichia coli*. J. Biol. Chem. *268*, 2307–2311. https://doi.org/10.1016/S0021-9258(18)53775-3.

68. Polikanov, Y.S., Blaha, G.M., and Steitz, T.A. (2012). How hibernation factors rmf, hpf, and yfia turn off protein synthesis. Science *336*, 915–918. https://doi.org/10.1126/science.1218538.

69. Häuser, R., Pech, M., Kijek, J., Yamamoto, H., Titz, B., Naeve, F., Tovchigrechko, A., Yamamoto, K., Szaflarski, W., Takeuchi, N., et al. (2012). Rsfa (ybeb) proteins are conserved ribosomal silencing factors. PLOS Genet. *8*, e1002815. https://doi.org/10.1371/journal.pgen.1002815.

70. Maki, Y., and Yoshida, H. (2021). Ribosomal hibernation-associated factors in escherichia coli. Microorganisms *10*, 33. https://doi.org/10.3390/microorganisms10010033.

71. Shimada, T., Yoshida, H., and Ishihama, A. (2013). Involvement of cyclic amp receptor protein in regulation of the rmf gene encoding the ribosome modulation factor in escherichia coli. J. Bacteriol. *195*, 2212–2219. https://doi.org/10.1128/JB.02279-12.

72. Graham, M.Y., Tal, M., and Schlessinger, D. (1982). lac transcription in Escherichia coli cells treated with chloramphenicol. J. Bacteriol. *151*, 251–261. https://doi.org/10.1128/jb.151.1.251-261.1982.

73. Grossman, A.D., Ullmann, A., Burgess, R.R., and Gross, C.A. (1984). Regulation of cyclic AMP synthesis in Escherichia coli K-12: effects of the rpoD800 sigma mutation, glucose, and chloramphenicol. J. Bacteriol. *158*, 110–114. https://doi.org/10.1128/jb.158.1.110-114.1984.

74. Guo, Y., and Amir, A. (2021). Exploring the effect of network topology, mrna and protein dynamics on gene regulatory network stability. Nat. Commun. *12*, 130. https://doi.org/10.1038/s41467-020-20472-x.

75. Lempp, M., Farke, N., Kuntz, M., Freibert, S.A., Lill, R., and Link, H. (2019). Systematic identification of metabolites controlling gene expression in E. coli. Nat. Commun. *10*, 4463. https://doi.org/10.1038/s41467-019-12474-1.

76. Chakraborty, P., and Ghosh, S. (2021). Emergent correlations in gene expression dynamics as footprints of resource competition. Eur. Phys. J. E Soft Matter *44*, 131. https://doi.org/10.1140/epje/s10189-021-00122-w.

77. Ro, C., Cashel, M., and Fernández-Coll, L. (2021). The secondary messenger ppgpp interferes with camp-crp regulon by promoting crp acetylation in *Escherichia coli*. PLOS One *16*, e0259067. https://doi.org/10.1371/journal.pone.0259067.

78. Zhao, L., Zhou, S.Y., Fu, Y., Shen, J.L., Yin, B.C., You, D., and Ye, B.C. (2024). A dual program for crp-mediated regulation in bacterial alarmone (p)ppgpp. mBio *15*, e0243024. https://doi.org/10.1128/mbio.02430-24.

79. Jishage, M., Kvint, K., Shingler, V., and Nyström, T. (2002). Regulation of sigma factor competition by the alarmone ppgpp. Genes Dev. *16*, 1260–1270. https://doi.org/10.1101/gad.227902.

80. Mauri, M., and Klumpp, S. (2014). A Model for Sigma Factor Competition in Bacterial Cells. PLOS Comput. Biol. *10*, e1003845. https://doi.org/10.1371/journal.pcbi.1003845. https://pmc.ncbi.nlm.nih.gov/articles/PMC4191881/.

81. Colland, F., Barth, M., Hengge-Aronis, R., and Kolb, A. (2000). Sigma factor selectivity of escherichia coli rna polymerase: role for crp, ihf and lrp transcription factors. EMBO J. *19*, 3028–3037. https://doi.org/10.1093/emboj/19.12.3028.

82. Melamed, S., Peer, A., Faigenbaum-Romm, R., Gatt, Y.E., Reiss, N., Bar, A., Altuvia, Y., Argaman, L., and Margalit, H. (2016). Global mapping of small rna-target interactions in bacteria. Mol. Cell *63*, 884–897. https://doi.org/10.1016/j.molcel.2016.07.026.

83. Zhang, Q., Brambilla, E., Li, R., Shi, H., Cosentino Lagomarsino, M., and Sclavi, B. (2020). A decrease in transcription capacity limits growth rate upon translation inhibition. mSystems *5*, e00575-20. https://doi.org/10.1128/msystems.00575-20.

84. Hueck, C.J., and Hillen, W. (1995). Catabolite repression in bacillus subtilis: a global regulatory mechanism for the gram-positive bacteria? Mol. Microbiol. *15*, 395–401. https://doi.org/10.1111/j.1365-2958.1995.tb02252.x.

85. Krásný, L., and Gourse, R.L. (2004). An alternative strategy for bacterial ribosome synthesis: *Bacillus subtilis* rRNA transcription regulation. EMBO J. *23*, 4473–4483. https://doi.org/10.1038/sj.emboj.7600423.

86. Matamouros, S., Gensch, T., Cerff, M., Sachs, C.C., Abdollahzadeh, I., Hendriks, J., Horst, L., Tenhaef, N., Tenhaef, J., Noack, S., et al. (2023). Growth-rate dependency of ribosome abundance and translation elongation rate in Corynebacterium glutamicum differs from that in Escherichia coli. Nat. Commun. *14*, 5611. https://doi.org/10.1038/s41467-023-41176-y.

87. Cooper, S., and Helmstetter, C.E. (1968). Chromosome replication and the division cycle of escherichia coli B/r. J. Mol. Biol. *31*, 519–540. https://doi.org/10.1016/0022-2836(68)90425-7.

88. Bremer, H., and Churchward, G. (1977). An examination of the cooper-helmstetter theory of dna replication in bacteria and its underlying assumptions. J. Theor. Biol. *69*, 645–654. https://doi.org/10.1016/0022-5193(77)90373-3.

89. Bachmann, B.J. (1990) Linkage Map of Escherichia coli k-12, [Eighth Edition]. Microbiol. Rev. 54, 130–197. https://doi.org/10.1128/mr.54.2.130-197.1990. Erratum in: (1991 Mar). Microbiol. Rev. 55, 191. https://doi.org/10.1128/mr.55.1.191-191.1991.

STAR★METHODS

KEY RESOURCES TABLE

REAGENT or RESOURCE	SOURCE	IDENTIFIER
Bacterial and virus strains		
NCM3722	Yale Depository	Strain ID: CGSC# 12355
Chemicals, peptides, and recombinant proteins		
Doxycycline (hyclate)	Sanbio	Cat# 14422-1
Ammonium acetate	Biosolve	Cat 0001244146BS
Acetic acid	Biosolve	Cat# 0001074131BS
Acetonitrile	Biosolve	Cat# 0001204102BS
Methanol absolute	Biosolve	Cat# 0013684102BS
Trehalose	Sigma-Aldrich	Cat# 27001-500ml
Ammonium hydroxide	Honeywell	Cat# 221228-100ml
Formic acid	Sigma-Aldrich	Cat# 27001-500ml-R
ppGpp (14-N chemical standard)	Trilink	Cat# N-6001-5
cAMP (14-N chemical standard)	Sigma-Aldrich	Cat# A6885
Ammonium chloride 15-N	CORTECNET	Cat# CN80P10
L-Aspartic Acid-15N	CORTECNET	Cat# CN350P025
L-Glutamic Acid-15N	CORTECNET	Cat# CN900P025
Tween-20	Bio-Rad	Cat# 1706531
Critical commercial assays		
1 mL/30 mg Oasis Wax cartridge	Waters	Cat.# 186002489
Durapore Membrane Filter, PVDF, 25mm	Merck Millipore	Cat.# HVLP02500
Deposited data		
Data published in this work	10.5281/zenodo.18097448	N/A
Recombinant DNA		
p*relA**	This study	AddGene ID: 175590
p*YFP*	This study	AddGene ID: 175592
Software and algorithms		
MATLAB R2020a	MathWorks	N/A
Custom Python Analysis and Plotting	10.5281/zenodo.18097448	N/A
MassHunter 7.0	Agilent	N/A
Other		
SeQuant ZIC-cHILIC 3um, 100Å, PEEK coated HPLC column, 100mm x 2.1mm	Merck Sigma	Cat# 1506570001
SeQuant ZIC-cHILIC Guard, PEEK coated guard column, 20mm x 2.1mm	Merck Sigma	Cat# 150436

EXPERIMENTAL MODEL DETAILS

Strains and plasmids

All experiments were performed using Escherichia coli wild-type strain NCM3722 (CGSC# 12355) and its derivative carrying a RelA* overexpression plasmid (pRelA*). pRelA* (Tet promoter, kanamycin resistance, sc101** origin) encodes a fusion of the N-terminal 455 amino acids of the E. coli RelA with mVenus as described in Buke et al.[61] and is available from the Addgene plasmid repository (Plasmid #175590).

Culture conditions

Cultures were maintained as described in Noga et al.[42] Cells were inoculated from a LB agar plate into 3 mL overnight cultures of the corresponding medium to be used the next day. Main cultures were prepared in 250 mL Erlenmeyer flasks containing at least 25 mL of fresh MOPS minimal medium supplemented with 0.2% (w/v) carbon source, which could be glucose, succinate, glycerol, acetate, aspartate or glutamate. Cultures with the pRelA* plasmid also contained 25 μg/mL kanamycin. (See resource table for reagents list.) Main cultures were inoculated from overnight precultures to 1/100 of the culture volume. Flasks were maintained at 37 °C in a Grant Instruments Sub Aqua Pro dual water bath and contained a 12-mm-long magnetic stir bar (VWR) coupled to a submerged magnetic stir plate (2mag MIXdrive 1 Eco and MIXcontrol 20) set at 300 rpm. To enable discrimination of cellular ppGpp and cAMP from the internal standard, the medium contained isotopically labeled $^{15}NH_4$ Cl or ^{15}N labeled aspartate or glutamate as nitrogen sources.

METHOD DETAILS

Sample collection and analysis for ppGpp and cAMP quantification

Samples were collected and processed largely as described in Buke et al.[61] For ppGpp titration, bulk cultures were induced with doxycycline at an optical density (600 nm) of 0.05-0.08 (early exponential phase). For each condition, three sampling replicates were collected. Samples were harvested at OD ∼0.35 for wild-type strains, while samples from induced pRelA* cultures were sampled only after growth rate stabilized (steady-state was defined as a variation of less than 10% in growth rate over a 30-minute period), which required between 3-5 hours. In all cases samples were taken between 0.3 and 0.4 OD. Three technical replicates were sampled by pipetting 1mL or 2.5mL (for lower ppGpp concentrations) of culture onto a wet filter under vacuum. The filter was immediately quenched upside down in 1mL ice-cold 2M formic acid. After filtering, a known concentration of the nucleotides of interest was added to the quenching solution. After 30 minutes in this solution, the filter was thoroughly washed and discarded. 25μL ammonium hydroxyde was added to the collected quenching solution in a 1mL tube which was frozen at -80 °C and was kept at least overnight and up to one month.

Growth rate measurements

Growth rates were quantified by continuously monitoring culture turbidity with an automated absorbance measurement system using a spectrophotometer (SPECTROstar Nano, BMG Labtech). Liquid culture from the 37 °C water bath flasks was continuously circulated through a flow-through cuvette (Starna Cells spectrophotometer flow cuvette 583.4-Q-10/Z8.5) using a peristaltic pump (Fisher Scientific GP1000). Optical density was measured every 5 s to 1 min, depending upon the growth rate. Growth rates were calculated by smoothing OD measurements with a 5-min wide Gaussian filter and computing the median of the time derivative of the natural logarithm of OD over a 1-h sliding window to precisely determine steady-state growth rates.

ppGpp and cAMP quantification via LC/MS

To measure nucleotides, samples were thawed on ice, then sonicated in ice-cold water for 10 minutes. Solid phase extraction was performed to purify nucleotides and get rid of other compounds that might cause matrix effects on the compounds of interest by altering the chromatographic separation or suppressing their ionization. To do so, during sonication, an Oasis Wax SPE cartridge 30mg 30μm was prepared by, first, flowing through three times 1mL methanol, then, three times 1mL 4.5 pH 50mM ammonium acetate. The sample was then applied on the cartridge and slowly flowed through. The cartridge was washed with 1mL 4.5 pH 50mM ammonium acetate followed by 1mL methanol and left to dry under vacuum for 5 minutes. The sample was eluted very slowly from the cartridge into an Eppendorf tube with 200μL 5:3:1:1 MeOH:ACN:H2O:NH4OH. The obtained sample was concentrated using a vacuum centrifuge after addition of 10μL of 5% trehalose for stabilization during drying. Once dried, the sample pellet was rediluted in 20μL 5:3:2 MeOH:ACN:H2O, then analyzed with an Agilent triple quad mass spectrometer and a ZIC-cHILIC column. For the first minute we maintained 90% mobile phase B 11.25mM ammonium acetate, 3.75mM acetic acid and 2mM acetylacetone in 80% ACN and 10% mobile phase A 3.75mM ammonium acetate, 1.25mM acetic acid and 2mM acetylacetone in water. Then we applied a gradient towards reaching 80% mobile phase A at 15 minutes. We maintained this concentration for one minute before applying a new gradient towards 100% mobile phase B between 16 and 18 minutes. We maintained this concentration until 22.5 minutes to flush out remaining compounds. For each compound, 14N and 15N peaks were obtained, corresponding respectively to the added standard concentration and the biological sample. Concentrations in pmol/OD600 were obtained by multiplying the 15N/14N area ratio by the added compound concentration, then normalizing by OD600 at sampling. The OD600 value was determined as the average of the last measurement before sampling and the first measurement after sampling. Error bars represent standard errors reflecting variability across technical replicates.

QUANTIFICATION AND STATISTICAL ANALYSIS

Conversion of growth rates into ribosomal fractions and elongation rates

To convert our growth rate data (Figure S1) into ribosomal fractions, we applied a linear fit to the total RNA/protein ratio measurements r from Zhu and Dai,[37] leveraging the conservation of the ribosomal growth law (Figure S2A):

$$r(\lambda) = q + m\lambda, \quad \text{(Equation 15)}$$

with $q = 0.073$ and $m = 0.217h$. We note that interpolating data from Dai et al.[47] yields substantially the same coefficients q and m. To obtain the "extended" ribosomal fraction, we then transformed RNA/protein ratios with the following conversion:

$$\phi_R = z \cdot r, \quad \text{(Equation 16)}$$

with $z = 0.76$, as discussed in Scott et al.[6].

To convert our growth rate data into elongation rate values, we leveraged the conservation of the elongation rate growth law under RelA overexpression[37] (Figure S2B) and computed

$$\varepsilon = \varepsilon_{max} \frac{r(\lambda)}{r(\lambda) + k_M}, \quad \text{(Equation 17)}$$

with $\varepsilon_{max} = 6.44h^{-1}$ (equivalent to 22 amino acids/s, see Methods S1) and $k_M = 0.11$ as in Dai et al.[47]. Note that Figure 4 is independent of the value we choose for ε_{max}, as only the ratio $\frac{\varepsilon_{max}}{\varepsilon}$ appears in the definition of the x-axis.

The knowledge of the relationships $\varepsilon(\lambda)$ and $\phi_R(\lambda)$ allows us to compute $f_a = \frac{\lambda}{\varepsilon \phi_R}$ for each data point in this study.

Generating the wild-type active ribosomes-ppGpp curve (Figure 5)

To generate the wild-type gray curves in Figure 5B and Figure 5C, we first fitted a linear relationship between ϕ_R and ppGpp (following ref. [20]), $\phi_R = c_0 \frac{1}{g}$, as in Figure 2B. The quantities λ and ϵ can be obtained from ϕ_R by inverting Equations 15,16 and 17 found in the previous paragraph. This allows us to express $f_a = \frac{\lambda}{\varepsilon \phi_R}$ as a function of ppGpp (Figure 5B). The wild-type curve in Figure 5C can be computed from f_a and ϕ_R through the relation $\phi_R^{in} = \phi_R(1 - f_a)$.

Modeling – coarse grained promoter strengths

To define the coarse-grained sector strengths in Equation 5, we start from Equation 3, and sum over the genes belonging to the same sector, leading to the coarse-grained messenger dynamics

$$\frac{d[m_I]}{dt} = \sum_{j \in I} k_j(\{r\}) [G_j] [N_{av}] - (\delta + \lambda)[m_I]. \quad \text{(Equation 18)}$$

We define the coarse-grained "sector strengths", as

$$\beta_I := \sum_{j \in I} k_j, \quad \text{(Equation 19)}$$

which gives Equation 5 if all genes are assumed to be present at the same concentration $[G]$.

Modeling – gene dosage effects

To incorporate gene dosage effects in our model, we express gene concentrations relative to the origin of replication (Ori), $[G_i] = d_i(\lambda, x_i)[Ori]$, with the dose d_i depending on the normalized distance x_i between gene and Ori, with the replication terminus (Ter) corresponding to $x = 1$.[31,87,88] For each sector, we can define a "regulatory activity", consistently with the terminology of Balakrishnan et al.,[31] as

$$\theta_I := \sum_{j \in I} k_j(\{r\}) d_j(x_j, \lambda). \quad \text{(Equation 20)}$$

Using this definition, we obtain an equation describing the transcripts dynamics for each sector:

$$\frac{d[m_I]}{dt} = \theta_I [Ori] [N_{av}] - (\delta + \lambda)[m_I], \quad \text{(Equation 21)}$$

which incorporates both transcription factor regulation and gene dosage effects.

In fast growth conditions, the relative abundance of genes located near the origin of replication tends to increase, enhancing the expression of certain genes, such as those encoding ribosomal proteins and ribosomal RNA.[89] To include this in our model, we use a mean-field approximation by assigning each gene in a given sector to a single chromosomal position x_I, thus writing $\theta_I = d(x_I, \lambda) \sum_{j \in I} k_j$. To obtain the parameters in Table S1, we set $x_R = 0.25$, and $x_P = 0.6$, reflecting the advantage at fast growth for ribosomal genes (see Methods S1 for details on how these values were estimated). This approximation leads to the factorization

$$\theta_I = \beta_I d(x_I, \lambda), \quad \text{(Equation 22)}$$

which separates the influence of transcription factors from gene dosage effects. With this setting, one still finds Equation 6, but with the definition

$$\omega_I := \frac{\theta_I}{\sum_J \theta_J}. \quad \text{(Equation 23)}$$

Methods S1 provides the full mathematical formulation of the model variant that includes gene dosage effects, which we used to replicate the data analyses and parameter fitting described in the main text. As already described by Balakrishnan et al.,[31] gene dosage effects are small in the range of conditions explored in this study ($0.2 - 1h^{-1}$). This model variant can be mapped onto the simplified version used in the main text by assuming the same gene copy number for all sectors (e.g., by setting $x_I = 0.5$ for all I). This leads to:

$$\omega_I = \frac{\theta_I}{\sum_J \theta_J} = \frac{\beta_I}{\sum_J \beta_J}, \quad \text{(Equation 24)}$$

which then gives Equation 7 in the steady state.

Fitting the model of transcriptional competition to ribosomal fractions

Data fitting of ribosomal fractions was performed through Orthogonal Distance Regression. A detailed explanation of the fitting approach can be found in Methods S1. Although we did not perform comparative modeling, we can assess the goodness of fit for our model in Figure 3A by calculating a coefficient of determination. Specifically, we compared a linear model that uses our growth rate prediction (based on ppGpp and cAMP concentrations for each condition as inputs) as the explanatory variable against the measured growth rate. The results are shown in Table S1, and visualized in Figure S3A for the model used in the main text (without gene dosage effects).

Transcriptional competition theory for hibernation factors

To explain the deviations in f_a as a function of ppGpp (Figure 5), we focused on ribosome hibernation factors. We group these factors into a new sector characterized by a mass fraction ϕ_{HIB} and a regulatory activity θ_{HIB}. We assume that hibernation factors are in competition with P and R, and use the same ϕ_Q and ϕ_{max} of the three sector model: Equation 7 for the hibernation sector reads

$$\omega_{HIB} = \frac{\theta_{HIB}}{\theta_{TOT}} = \frac{\theta_{HIB}}{\theta_R + \theta_P + \theta_{HIB}}\phi_{max} \approx \frac{\theta_{HIB}}{\theta_R + \theta_P}\phi_{max}, \quad \text{(Equation 25)}$$

where we neglect the term θ_{HIB} at the denominator given the small size of the hibernation sector, based on the proteomics data in ref. [9]. At steady-state $\omega_{HIB} = \phi_{HIB}$ due to Equation 7, and ignoring gene dosage effects, we find from the above equation

$$\phi_{HIB} = \frac{\beta_{HIB}(\cdot)}{\beta_R(g) + \beta_P(c)}\phi_{max}.$$

Specializing this equation to points A and B in Figure 5D leads to Equation 14 of the main text.

Definition of regulatory sectors for model–proteomics comparison

To compare our model with the proteomics data from Zhu et al.[38] and Zhu et al.,[39] we identified genes regulated by ppGpp and cAMP using the databases RegulonDB[58] and EcoCyc.[59] These resources provide information on transcription factors, their target genes, and the corresponding modes of regulation (activation or repression). Genes with ambiguous regulatory annotations were excluded from the analysis. We then examined the distribution of cAMP–CRP and ppGpp–DksA target genes across proteome sectors. For this purpose, we adopted the framework of Mori et al.,[9] in which proteins are partitioned into sectors based on their expression changes under anabolic, catabolic, or translational limitation, as determined from proteomics data. This approach defines $2^3 = 8$ proteome sectors, including the anabolic, catabolic, and ribosomal sectors (Figure S5).

To ensure a robust analysis, we defined the cAMP-activated sector as the set of genes for which cAMP–CRP can be considered among the main activators; specifically, genes activated by cAMP–CRP according to RegulonDB and upregulated under catabolic limitation according to Mori et al.[9] Genes downregulated under C-LIM were excluded, as this downregulation cannot be explained by cAMP-mediated effects. Similarly, the ribosomal sector was restricted to structural ribosomal proteins, excluding affiliated proteins, because their relationship to growth rate under RelA overexpression has not been fully characterized. The parameter ϕ_{max} was adjusted to reflect these choices (Figure S5; Table S1). We then used the wild-type linear growth law for the restricted ribosomal sector (Figure S5D, green line), derived from the proteomic data in Mori et al.,[9] to convert growth rates into restricted ribosomal fractions, analogously to Eq. 15. We then compared the model, defined with the updated parameters ϕ_{max}, q and m, to our data, obtaining the fitted parameters μ_1, μ_2, μ_3 (Table S1).